Seznam vlastních publikací, Jakub Cejpek

- **2018**

Cejpek J. Design of composite landing gear for an LSA airplane

Aircraft Engineering and Aerospace Technology, ISSN: 0002-2667, SNIP=0.580, SJR=0.273

Volume 90, 2018 - Issue 4

- **2016**

Cejpek J., Juračka J., Modifications of a simple I-beam and its effects on the stress state

Aviation, ISSN: 1648-7788, SNIP=0.457, SJR=0.188

Volume 20, 2016 - Issue 4

- **2015**

Weis M., Cejpek J., Juračka J. Acoustic Emission Localization in Testing of Composite Structures

Applied Mechanics and Materials, ISSN: 1662-7482

Volume 821, 2016

- **2013**

Cejpek J. Napěťově-deformační analýza segmentu kompozitového křídla

Příspěvek na konferenci „Setkání uživatelů MSC.Software s.r.o. 2013“

Setkání uživatelů MSC.Software s.r.o. 2013. ISBN: 978-80-260-4173- 3.

- **2012**

Cejpek J., Mališ M., Urík T. Application of filament winding technology for CS22 category wing construction

Příspěvek na konferenci „READ 2012“

Research bulletin, ISSN: 1425- 2104.

2018

Design of composite landing gear for an LSA airplane

Aircraft Engineering and Aerospace Technology, ISSN: 0002-2667, SNIP=0.580, SJR=0.273

Volume 90, 2018 - Issue 4

Emerald Aircraft Engineering and Aerospace Technology: An International Journal

Design of composite landing gear for an LSA airplane

Journal:	*Aircraft Engineering and Aerospace Technology*
Manuscript ID	AEAT-11-2016-0216.R2
Manuscript Type:	Research Paper
Keywords:	Beam Element, LSA, Composite, Landing Gear, Spring

Design of composite landing gear for an LSA airplane

Abstract

Purpose

The purpose is to introduce a software tool under development by the author. Based on industry demands a software tool is developed to fill the gap between commercial software and limited closed-form analysis in this specific area.

Design/methodology/approach

Python programming language offers a great potential to develop relatively simple software that includes GUI and can be turned into an executable file – therefore easily spread. Also, thanks to large community, Python offers extended scientific libraries for solving number of engineering problems.

Results are compared to the commercially available software (in this case, MSC NASTRAN). Further evaluation is to compare results to the laboratory tests.

Findings

First results were obtained on the comparison between KuFEM and NASTRAN. These results are sufficient reassurance for next stages of development.

Next results are the comparison of KuFEM results to the laboratory test. As only one type of product has been tested, no final conclusion can be made. However within these limits, the results are very promising and optimistic.

Research limitations/implications

Future development will include:

- further evaluation on different products,
- even more composite-oriented calculations,
- enhanced graphical environment.

Practical implications

KuFEM, within its limits is an alternative to other commercial programs. It is meant to compromise between limited closed form designs and detailed designs in expensive software.

Social implications – this is an optional entry.

Originality/value

KuFEM is a unique software tool. It allows user to work with finite element method in a simple pre-programmed way. It enhances the standard BEAM elements in order to go deeper in the analysis. Currant evaluation promises potential good results.

Keywords Beam Element, LSA, Composite, Landing Gear, Spring.

Paper type Research paper.

Introduction

When designing new light sport airplane with fixed landing gear, the manufacturer faces a question whether to buy a final product (such as those offered by ComLet company [4]), or make his own design.

Designing own composite landing gear can be approached with large commercial FEA packages (such as Nastran, Ansys, Abaqus, etc.), use CAD built-in analysis modules or do it with closed form analysis on a sheet of paper.

These closed—form solutions may be fast and simple, but they offer only little precision and the final product is more question of designer's feeling, trial-and-error experimenting and possibly some reverse engineering.

On the other hand using expensive software packages may give great results but requires time and experienced user. The most time consuming stage of the design is modelling different layups and analyse the results.

This paper presents option in between. Simple program with its own Graphical User Interface (GUI) capable of predicting deformed shape, strains and stresses of the landing gear.

State of the art and motivation

At present day, the author works for a small company based in Olomouc, Czech Republic. The company's name is TechProAviation and the main article of production is metal light sport airplanes. Design, manufacturing and certification of several types have finished or are still going on.

Even though the airframe is made out of aluminium alloy, there are few composite parts. Wingtips and cockpit parts for sure. But most importantly: landing gear and springs.

Main landing gear, nose wheel spring or tail gear spring are classified as thick composite parts, made mostly out of unidirectional composite material. The current trends in composite landing gear were studied with a conclusion, that a new software tool needs to be developed.

Mister Spencer [8] describes a procedure of design and optimization of a composite landing gear by means of NASTRAN solution sequence SOL200. He suggests using rectangular beam elements, and optimizing their parameters in iterative way.

Mr. Goyal [9] stresses out the importance of kinematics (the influence of the deformed shape on the stresses). Because of achieving large deformations, he suggests to use non-linear analysis techniques. An example design is shown in the article. The aim is to design composite main landing gear for a light sport airplane of m_{TOW} = 350kg. The non-linear analysis, employed by mr. Goyal, applies the loading gradually in different sub-steps.

Ms. Ilic [10] describes the development of the main landing gear for an unmanned aerial vehicle. First, the global geometry is defined. Along the length a total of 8 control points are chosen. In these points the strains are evaluated and compared to strain gages reading from the laboratory test. The numerical analysis used 2D shell elements with 2D orthotropic material definition.

Mr. Torstenfelt [11] explains the principles of finite element method in very understandable fashion. First bars are explained and the equations are derived. Then the same is shown for beams. Examples are given for 2D and 3D cases. Also common mistakes are pointed out. The same topics are covered in a book from Mr. Ferreira [3]. As part of the book MATLAB codes are provided to the reader so he can see first-hand the procedure.

When building a model of some system, the validation and verification is necessary part of the development. Mr. Sargent: [13] defines these terms as follows:

- Model validation ensures that the model is used within its domain of applicability.
- Model verification ensures that the model and its implementation are correct.

Mr. Conover [7] used similar definition. In this text, author defines these terms in more straight forward manner:

- Model verification: KuFEM calculates results that are same or very close to NASTRAN.
- Model validation: KuFEM calculates results that are close to the real laboratory tests.

Very important topic is the material properties that will be used. Mr. Chamis [6] presented the significance of tensile / compression elastic moduli difference. He formulated modular ratio parameter that is a fracture of elastic modulus in

tension and compression. Should the modular ratio be 1.5, the deflection of three-point-bend loading can be 25% underestimated. This implies the importance to consider the difference.

Analysing the mathematical formulation [13] of unidirectional composite material, more usually referred to as transversely isotropic, the following Hook's law can be deduced:

$$\begin{Bmatrix} \epsilon_1 \\ \epsilon_2 \\ \epsilon_3 \\ 2\cdot\gamma_{23} \\ 2\cdot\gamma_{13} \\ 2\cdot\gamma_{12} \end{Bmatrix} = \begin{bmatrix} \frac{1}{E_1} & -\frac{\mu_{12}}{E_1} & -\frac{\mu_{12}}{E_1} & 0 & 0 & 0 \\ -\frac{\mu_{12}}{E_1} & \frac{1}{E_2} & -\frac{\mu_{23}}{E_2} & 0 & 0 & 0 \\ -\frac{\mu_{12}}{E_1} & -\frac{\mu_{23}}{E_2} & \frac{1}{E_2} & 0 & 0 & 0 \\ 0 & 0 & 0 & \frac{2\cdot(1+\mu_{23})}{E_2} & 0 & 0 \\ 0 & 0 & 0 & 0 & \frac{1}{G_{12}} & 0 \\ 0 & 0 & 0 & 0 & 0 & \frac{1}{G_{12}} \end{bmatrix} \begin{Bmatrix} \sigma_1 \\ \sigma_2 \\ \sigma_3 \\ \tau_{23} \\ \tau_{13} \\ \tau_{12} \end{Bmatrix}$$

When analysing the actual numbers in the area of application intended for KuFEM, the Hook's law shrinks to an isotropic material:

$$\epsilon_1 = \frac{1}{E_1}\cdot\sigma_1$$

This is not true along the whole landing gear however. In the area of outer attachment a significant through-thickness is introduced (figure 4, left). In this area, σ_3 needs to be calculated.

Program KuFEM

This section introduces the GUI and explains the input user must make prior running the calculation. The program is primarily intended for the main landing gear – the explanation will use this geometry to illustrate the meaning of the data.

User should be aware of the meaning of the term *"mid-fibre"*. The mid-fibre is created as an intersection of two planes representing middle of the thickness and width. It is defined through nodes (points lying on the mid-fibre, figure 2). There can be as many nodes as the user defines. Four nodes have special meaning: point "L" (where the forces are introduced), point "D" (where the axle is attached to the laminate) and points "A" and "B" (where the landing gear is attached to the fuselage). These special points must be included in the input file and later be referred to by their number. All nods must be listed in order as shown on figure 2.

Program Input

There are two input files that KuFEM needs to run the calculation. Both are excel XLS or XLSX files in column-wise orientation.

First file describes the geometry of the mid-fibre. Each two following nodes define one element (the number of elements is one less than the number of nodes). Figure 2 shows landing gear geometry simplified into the nodes and elements.

The second input file is also an excel sheet. It lists the geometry and properties of each element. As the number of elements is not limited by the program, it is only up to user to set the reasonable amount. Two aspects must be considered: a) how many elements is user able to define sets the maximum, whereas b) the required accuracy sets the minimum.

Figure 1 Program GUI.

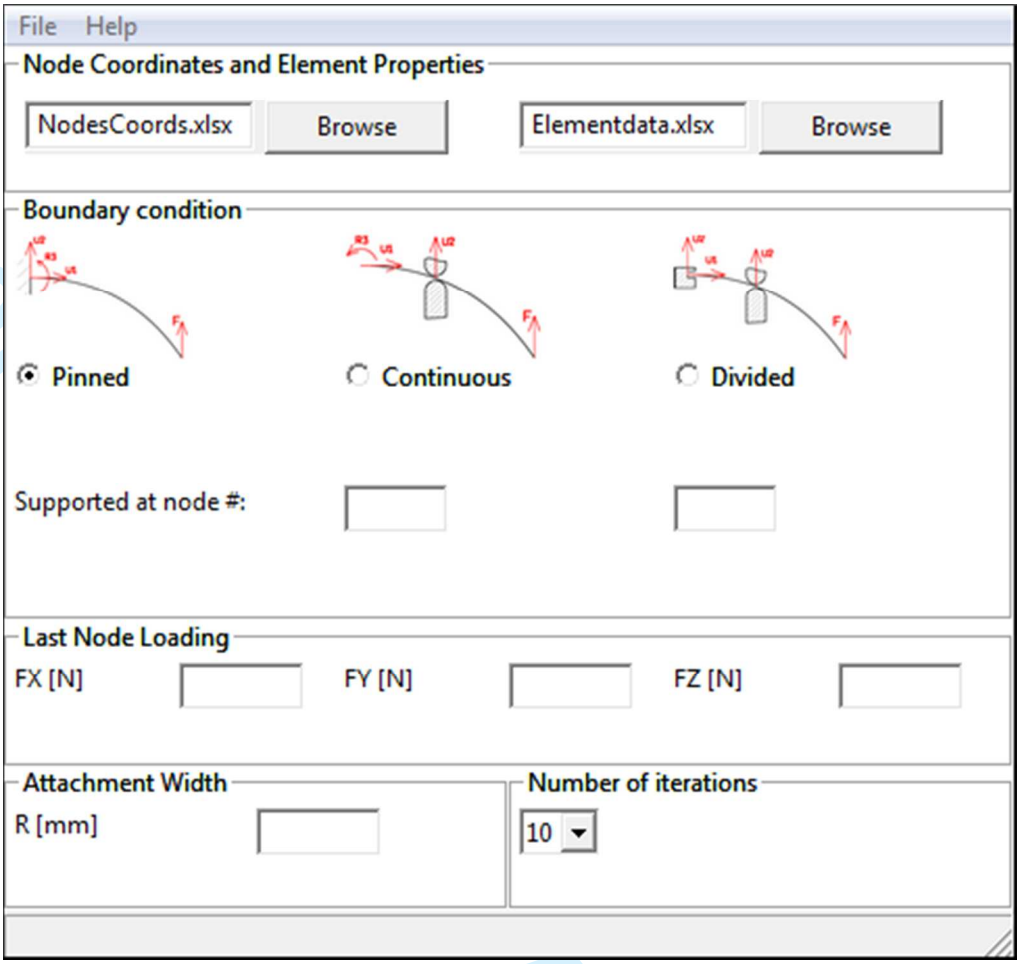

Figure 2 Iso-view on landing gear. Important points location and coordinate system orientation.

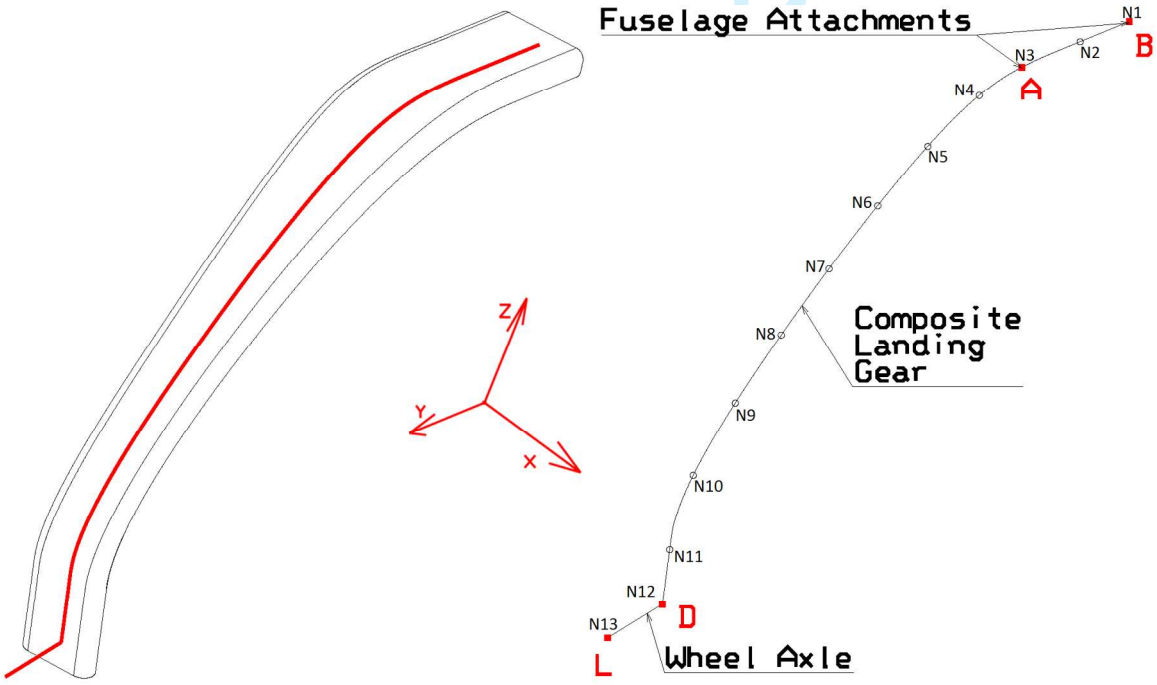

The geometry of the element includes the width and thickness (upper flange, lower flange, wrap and total thickness, dimensions explained in table 1). Also the upper and lower flange may have different mechanical properties, depending on tensile / compression loading [6]. In this example, the upper flange is compressed while the lower flange is stretched out.

Figure 3 Geometry of a cross-section.

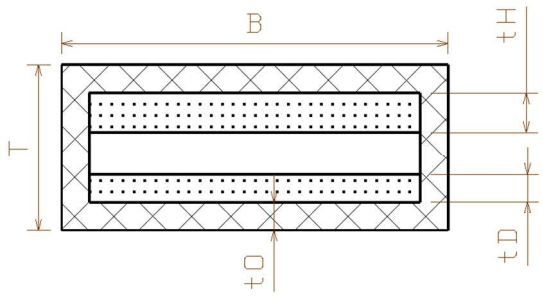

Table 1 Denotation of geometry.

T [mm]	total thickness (without wrap)	t_O [mm]	thickness of the wrap layers (constant all around)
B [mm]	total width (without wrap)	E_H [MPa]	upper flange modulus of elasticity
t_H [mm]	upper flange thickness	E_D [MPa]	lower flange modulus of elasticity
t_D [mm]	lower flange thickness		

Besides two excel sheets describing geometry and mechanical properties, user must fill information about boundary conditions and loading. These inputs are shown on the GUI window on figure 1. These inputs are:

- type of boundary condition and the number of supported node,
- three vectors of the loading force (figure 4, right),
- attachment geometry (figure 4, left),
- number of iterations.

Figure 4 Outer fuselage attachment geometry and force vectors.

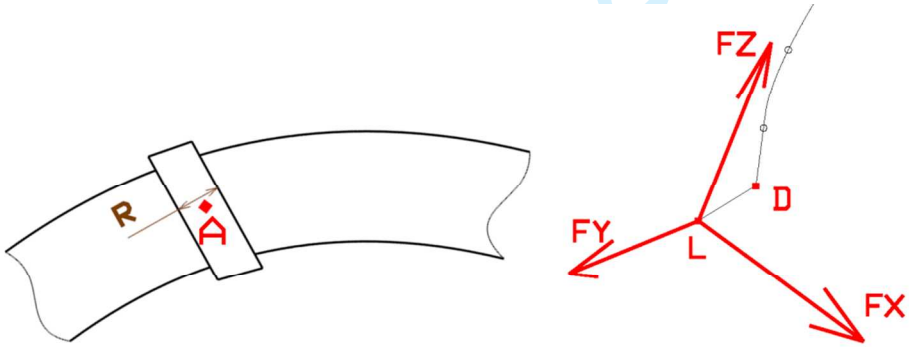

Deformed Shape Calculation

This calculation is based on an assumption, that the X-direction displacement is negligible in comparison to the Y and Z directions. Assuming UX=0 significantly reduces difficulty of the problem. Only two translations and one rotation for each node will be calculated.

For a two-dimensional beam problem the Euler-Bernoulli beam theory is adopted. It assumes that undeformed plane sections remain plane under deformation (cross-section remains constant).

Local stiffness matrix is calculated for each element:

$$LS = \begin{bmatrix} \frac{A \cdot E}{L} & -\frac{A \cdot E}{L} & 0 & 0 & 0 & 0 \\ -\frac{A \cdot E}{L} & \frac{A \cdot E}{L} & 0 & 0 & 0 & 0 \\ 0 & 0 & 12 \cdot \frac{E \cdot J}{L^3} & -12 \cdot \frac{E \cdot J}{L^3} & 6 \cdot \frac{E \cdot J}{L^2} & 6 \cdot \frac{E \cdot J}{L^2} \\ 0 & 0 & -12 \cdot \frac{E \cdot J}{L^3} & 12 \cdot \frac{E \cdot J}{L^3} & -6 \cdot \frac{E \cdot J}{L^2} & -6 \cdot \frac{E \cdot J}{L^2} \\ 0 & 0 & 6 \cdot \frac{E \cdot J}{L^2} & -6 \cdot \frac{E \cdot J}{L^2} & 4 \cdot \frac{E \cdot J}{L} & 2 \cdot \frac{E \cdot J}{L} \\ 0 & 0 & 6 \cdot \frac{E \cdot J}{L^2} & -6 \cdot \frac{E \cdot J}{L^2} & 2 \cdot \frac{E \cdot J}{L} & 4 \cdot \frac{E \cdot J}{L} \end{bmatrix}$$

Each element is positioned in a different angle α, relative to the YZ axis. In the next step a transformation matrix of goniometric functions is calculated:

$$T = \begin{bmatrix} cos\,(\alpha) & 0 & sin\,(\alpha) & 0 & 0 & 0 \\ 0 & cos\,(\alpha) & 0 & sins\,(\alpha) & 0 & 0 \\ -sin\,(\alpha) & 0 & cos\,(\alpha) & 0 & 0 & 0 \\ 0 & -sin\,(\alpha) & 0 & cos\,(\alpha) & 0 & 0 \\ 0 & 0 & 0 & 0 & 1 & 0 \\ 0 & 0 & 0 & 0 & 0 & 1 \end{bmatrix}$$

By multiplying these two matrixes for each element a global stiffness matrix is obtained:

$$[GS] = [T]^{-1} \cdot [LS] \cdot [T]$$

Combining all Global Stiffness matrixes together creates Global Stiffness of the whole Model (GSM). This is ruled by the DOF number for each node.

Those DOF that were removed by boundary conditions are reflected in the GSM matrix and also Loading Vector F. Final vector of displacements and rotations is obtained by multiplying the GSM matrix and Force vector:

$$\{U\} = [GSM] \cdot \{F\}^{-1}$$

Also the reactions can be determined by multiplying global stiffness matrix and transposed displacement vector:

$$\{R\} = [GSM] \cdot \{U\}^{T}$$

σ_1 and ε_1 stresses and strains

General FEM approach to determine stresses and strains is to solve strains through strain-displacement matrix [B] and then obtain the stresses by multiplying the strain vector by stiffness matrix:

$$\{\epsilon\} = [B]\{U\}$$

$$\{\sigma\} = [E]\{\epsilon\}$$

It represents a function of the partial derivatives of shape functions with respect to the global XYZ coordinate system. This leads to Jacobian introduction. Jacobian matrix relates derivatives of the function in local coordinate system to derivatives in global coordinate system.

However, for KuFEM this approach will be substituted by more intuitive approach, based on geometry and element forces. Suggested approach follows simple idea, familiar to all engineering students:

$$\frac{Force}{Area} \rightarrow Stress \quad and \quad \frac{Stress}{Stiffness} \rightarrow Strain$$

This approach has one more advantage. The first part of the calculation was considering only 2D case. This is not the limit of the suggested procedure however. It allows considering all six components of loading (3 forces and 3 moments, see figure 5).

Figure 5 Element geometry and loading in the centre of the element.

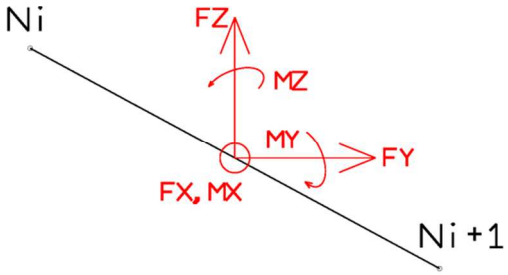

It has been described in previous section that the whole geometry is located in one plane; therefore the geometry is two dimensional. An angle between the element longitudinal axis $\vec{I}$ and global vertical axis $\vec{Z}$ can be calculated. According to this angle all forces and moments are transformed into the element coordinate system (figure 6).

Figure 6 Element geometry and element loading.

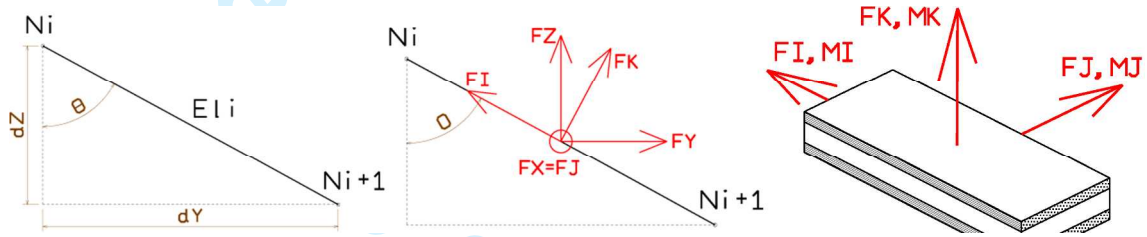

Based on geometrical characteristics and the element forces, the stresses are calculated. Primarily, the stress along the fibre in the flange is calculated as a sum of:

- bending along lateral axis: $\sigma_{1J} = \frac{M_J}{J_J} \cdot k$
- bending along vertical axis: $\sigma_{1K} = \frac{M_K}{J_K} \cdot j$
- normal tension/compression: $\sigma_{1I} = \frac{F_I}{A}$

Figure 7 Element geometry and loading example.

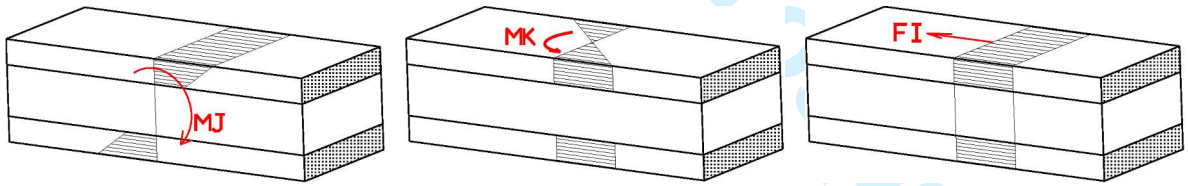

- total maximum stress in the fibre is calculated as a sum: $\sigma_1 = \sigma_{1J} + \sigma_{1k} + \sigma_{1I}$
- from Hook's law, the strain is obtained through the elastic modulus: $\epsilon_1 = \frac{\sigma_1}{E_1}$

Fuselage Attachment

The analysis is focused on the boundary conditions other than pinned. The outer fuselage attachment is extremely loaded with through thickness force as a result of the geometrical arrangement (figure 8, left). Also the twisting moment, created by FX is restrained here (figure 8, right).

Figure 8 left: influence lines of the landing gear, R_{AZ} force component, right: twisting moment from FX.

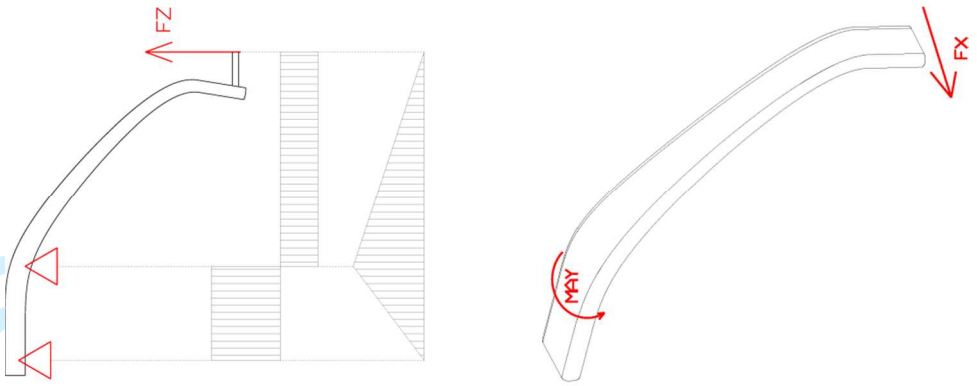

This through thickness force acts perpendicular to the fibres, therefore effectively decreasing the allowed values in direction along the fibres. Significant through-thickness stress leads to decreased strength capacity in direction 1. Using interactive failure criterions, Tsai-Wu [5] for example is recommended.

These failure criteria are not part of KuFEM. User is only provided by the calculated stresses and the failure criterion assessment is up to him or her and the material data available. Figure 9 illustrates the stress state in the area of fuselage outer attachment and failure envelope of an elliptical criterion as an example.

Figure 9 Through-thickness stress (σ_3) decreases allowed stress along the fibres (σ_1).

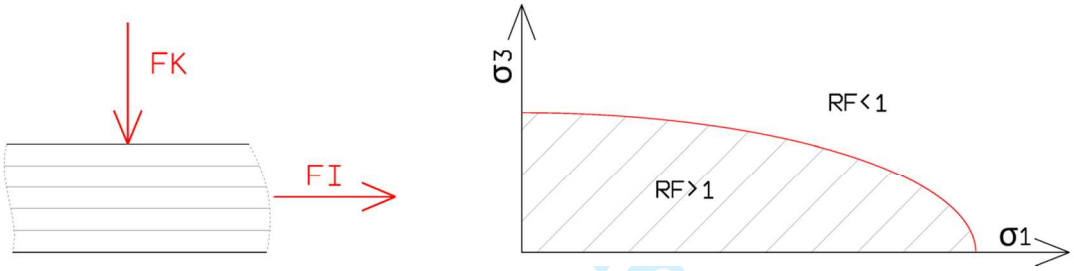

For evaluating the through-thickness stress, user has to input the value R (width of the attachment). Obviously, the wider the attachment is the lower the stress. The attachment geometry is important also. Figure 10 shows unsuccessful geometry of attachment.

Figure 10 Problematic attachment geometry.

Problematic of determining the failure index of the multi-axial stress state is complex task and beyond the purpose of this program. Therefore only the force and stress values are presented to the user.

The stress σ_3 (figure 11) presented consists from two separate forces. One is the vertical reaction to the F_Z force. The other is the reaction to the F_X induced twisting moment.

Figure 11 Components of σ_3 stress in outer attachment.

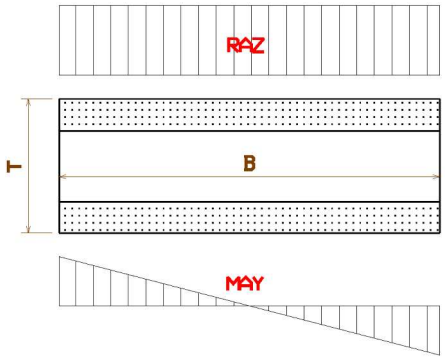

Vertical force reaction in outer hinge:

$$R_{AZ} = -F_Y \cdot \frac{2 \cdot A_Z - L_Z - B_Z}{A_Y - B_Y} - F_Z \cdot \frac{L_Y - B_Y}{A_Y - B_Y}$$

Moment reaction to the FX force:

$$M_{AY} = -F_X \cdot (A_Z - L_Z)$$

From these reactions the peak of the through thickness stress is calculated and presented to the user. Further evaluation is up to user's experience and available material characteristics. Finally the last analysis is the wrap shear stress determination:

$$\tau_O = \frac{F_K}{2 \cdot T \cdot t_O} + \frac{M_I}{2 \cdot B \cdot T}$$

Linear and non-linear calculation

In case of main landing gear large deformations are expected. For this reason user can choose using non-linear calculation. Non-linear calculation reflects progressive deformation as a response to the increasing load (figure 12).

User may choose between 1, 5, 10 and 20 iteration steps. Choosing 1 effectively means linear solution.

Figure 12 Difference between linear (1 step) and non-linear (2 steps) calculation.

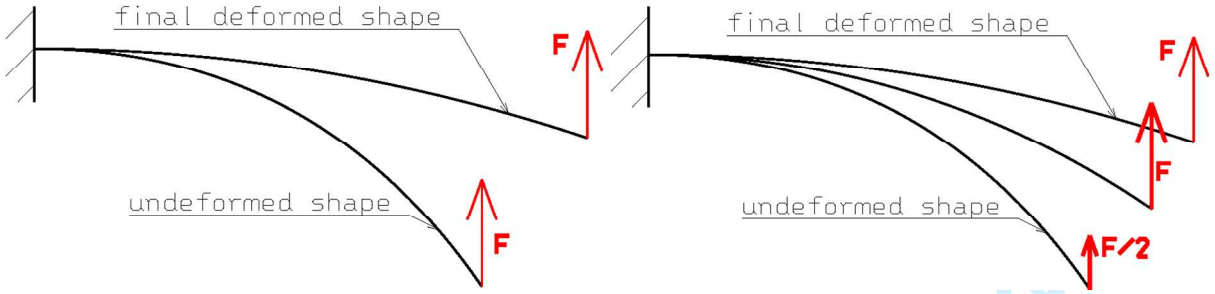

At this point, the functionality has not been finished. Preliminary verification suggests deeper understanding of the subject will be needed. The topic will not be discussed further in this article.

Program Run and Outputs

KuFEM has been created in Python programming language and is fully executable on any Windows platform (XP and newer, 32bit or 64bit). Program includes graphical user interface and provides data output in various forms.

Graphical User Interface and Data Input

Simple graphical user interface (shown on figure 1) allows user to define the loading, boundary condition, geometry, properties and choose number of iterations.

- Node coordinates

Browse for an excel sheet with [Y,Z] coordinates of the nodes.

- Element properties

Browse for an excel sheet with thickness, width and elastic moduli of each element. Number of elements must be one less than the number of nodes.

- Number of iterations

Select number of iterations. Choices are 1, 5, 10 and 20. If selected 1, linear calculation will be run (stiffer results will be obtained).

- Loading at last node

Define the forces in X,Y,Z direction acting in the middle of the wheel (point “L”).

- Boundary condition specification

Select the type of boundary condition (figure 13). Pinned is a single point fix: in node number 1 are removed all DOFs. If selected divided BC, user is required to define the node’s number, where is located the outer attachment to the fuselage. Node 1 (inner attachment to the fuselage) removes both translations, whereas the outer attachment at node specified by user only vertical translation is removed. Similar is continuous BC. User is also required to define number of node with the support. At node number 1 are symmetrical boundary condition (zero Y-displacement, zero X and Z rotation.

Figure 13 left: Pinned BC, centre: continuous BC, right: divided BC.

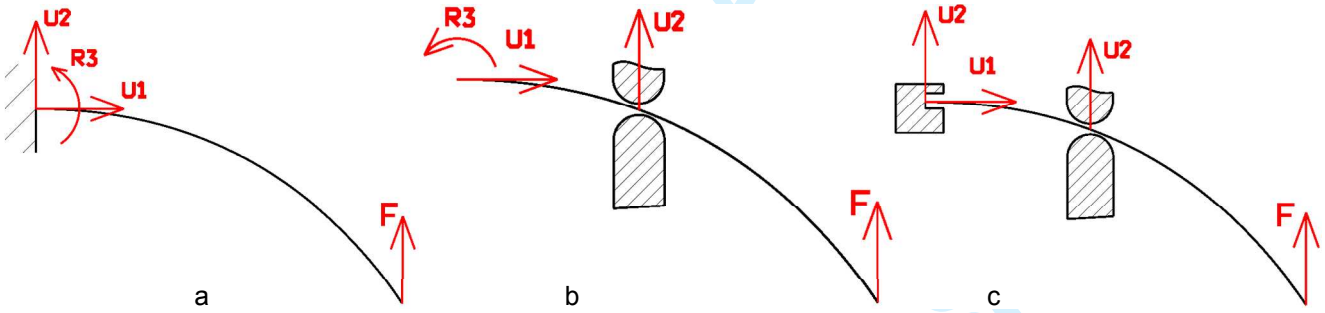

- Attachment

Specify the width of the outer attachment to the fuselage for through-thickness stress determination. This input is meaningless if pinned boundary condition selected.

Program Commands and Outputs

When all data are filled correctly, the user can execute the calculation and create output files afterwards. Figure 14 shows the command menu.

Figure 14 Available program commands.

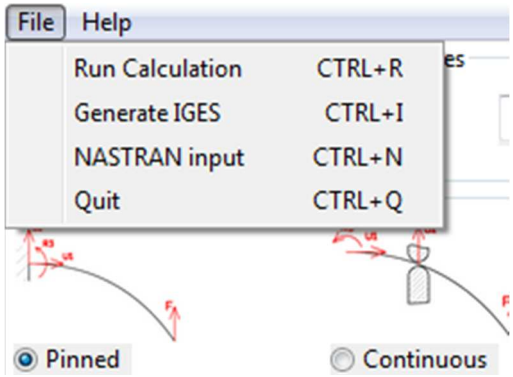

- Run Calculation

Runs the calculation and creates Excel and text outputs with stress strain data. User can later create graphs from this Excel outputs. Text output summarizes the results.

- Generate IGES

Deformed geometry is exported in IGES file (one of the universal 3D graphics format).

- NASTRAN input

Program can generate BDF file that can be run by standard NASTRAN solver.

Example problem

Latest work on KuFEM project concerns the nose wheel spring on Merlin 103 airplane (figure 15).

Figure 15 Merlin 103 nose wheel spring.

At first, loading and working diagram (figure16, left) has been given as a goal to be met. The loading is determined through the level landing at front centre of gravity position defined in [1], [2]. The travel of the

By using KuFEM program and simple spread sheet adjustments the geometry and layup has been optimized in order to meet the working diagram (figure 16, right) as best as possible. Linear and non-linear (10 iterations) solution is shown.

To compare results obtained in KuFEM, same task has been submitted into NASTRAN solver. Two models were analysed in NASTRAN (shown on figure 17):

1. Beam 1D model (equivalent to the KuFEM model, KuFEM itself generated source BDF file)
2. HEX 3D model (8-node HEX elements were used)

Figure 16 Required working diagram. KuFEM calculation.

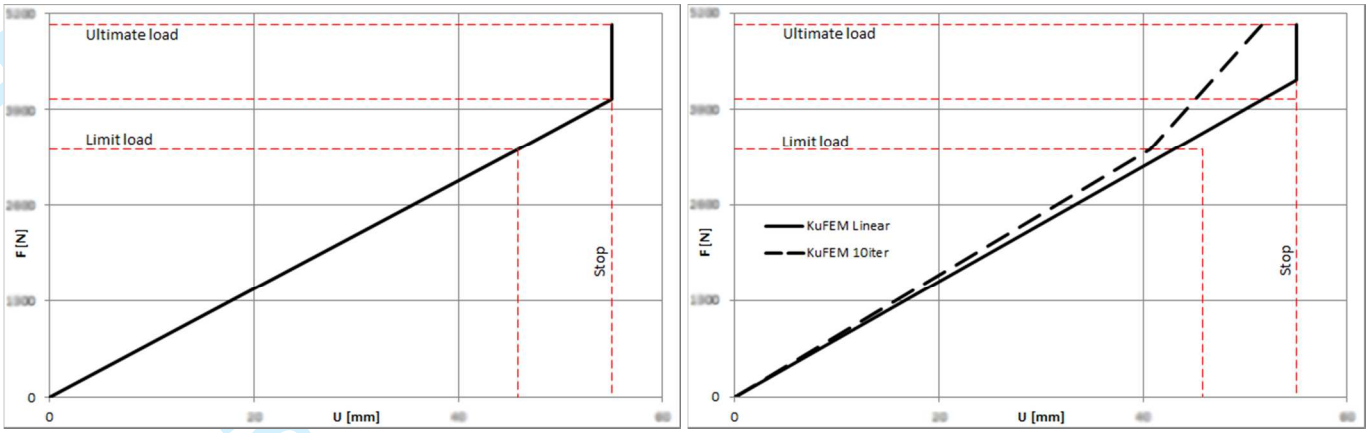

Figure 17 NASTRAN solution and models.

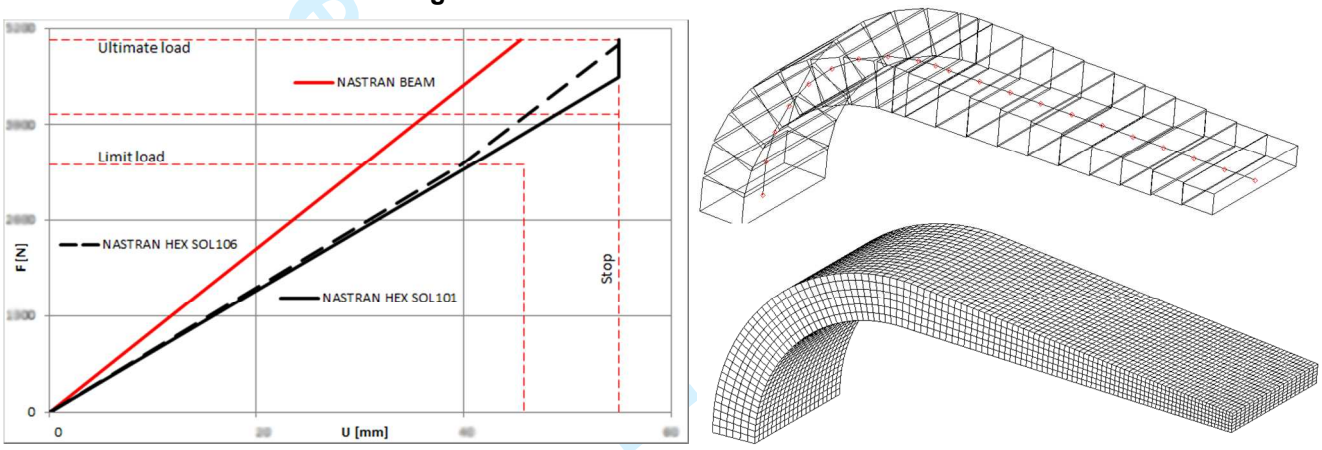

According to the calculated designed specification a series of springs has been manufactured. Three specimens were tested in laboratory. Total of nine measurements are evaluated as a sector in the working diagram on figure 18.

Figure 18 Laboratory tests results.

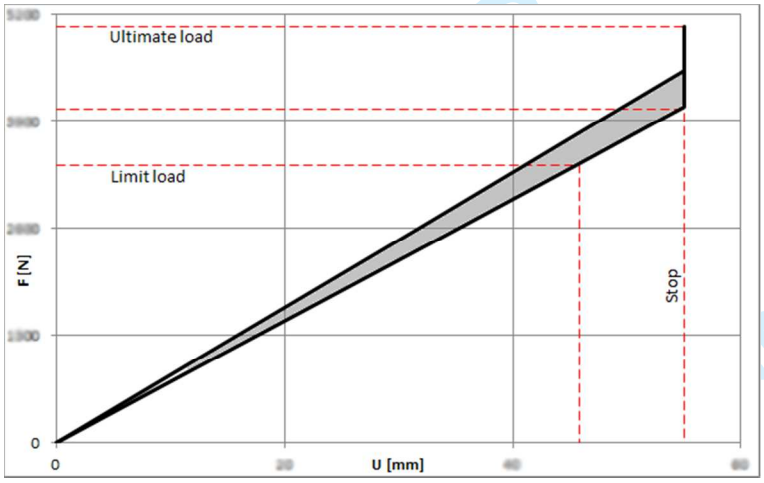

Conclusion

This article has introduced a software tool that aims to simplify the design stage of the composite component. KuFEM is designed to fill the gap between limited closed formula approach and sophisticated commercial CAE software.

A case study is presented on a real structure for the Merlin 103 airplane. Inputs and outputs were briefly explained, so was the mathematical apparatus.

The Merlin 103 nose spring gear has been designed using KuFEM. Further analysis made in NASTRAN confirmed the mathematical results. Also final products were tested in the laboratory. The only parameter that could be tested is the stiffness of the spring. All three results are in good agreement.

As the springs were not to be destroyed, the ultimate strength prediction could not be verified. However the stresses and strains obtained in KuFEM and NASTRAN are in agreement.

Mr. Conover [7] defined the terms verification and validation:

- Verification: *"Did I construct the models right?"*
- Validation: *"Did I construct the right models?"*

In these terms KuFEM has been verified to give the correct numbers based on comparison with NASTRAN results for both: linear displacement and stresses and strains.

As for validation, the nose gear spring test has proofed KuFEM to be valid in terms of displacement. Stresses and strains could not be validated – no strain gage measurement has been taken, nor has been reached the ultimate strength.

The author defines the following evaluation (table 2) criteria in order to compare the available solvers:

Table 2 Evaluation of the solutions (1=best, 3=worst).

	Closed formula	KuFEM	Commercial programs
Price	1	2	3
Experienced engineer	2	1	3
Speed	2	1	3
Result accuracy	3	2	1
Solution versatility	3	2	1

Last author's note concerns the purpose of the KuFEM software. It aims to help with design of the product. By no means is it intended as a proof-of-structure tool. Only the strength test can provide a valid proof.

Acknowledgments

This project is an initiative of the author of this paper. Author would like to thank to the TechProAviation, s.r.o. company for all the support and trust given to the author. The program can proof to be useful only with the hard laboratory data, provided by the company.

References

[1] ELSA-K: konsolidované znění, LAA ČR, 2011

[2] F 2245-07: Standard Specification for Design and Performance of a Light Sport Airplane, ASTM Int.

[3] Ferreira, A., MATLAB Codes for Finite Element Analysis, Solid Mechanics and its Applications, volume 157, University do Port, Portugal, ISBN: 978-1-4020-9199-5, 2009.

[4] ComLet e-shop, http://www.comlet.cz/, (June 18, 2016)

[5] Dávila, C., Camanho, P., Failure Criteria for FRP Laminates, Journal of Composite Materials, Vol. 39, 2005

[6] Chamis Ch., Analysis of three-point-bend tests for materials with unequal tension and compression properties. 36 pages. NASA technical note TN D-7572, 1974.

[7] Conover D., Verification and validation of FEA simulations, ANSYS presentation. 19 pages. Cornell University. 2008.

[8] Spencer E. A novel optimization strategy for composite beam type landing gear for light aircraft. 24 pages. United Technologies Aerospace Systems, [online 2016-12-16]

[9] Goyal A., Design, analysis and simulation of a composite main landing gear for a light aircraft. 6 pages. MSRSAS Bangalore. 2002.

[10] Ilic I., Strength analysis of main landing gear type layered composite leaf spring for unmanned aerial vehicle. 4 pages. Military Technical Institute, Belgrade. 2012.

[11] Torstenfelt B., Finite Elements, Preliminary edition LiU-IEI-S--08/535--SE. Linköping universitet. 2008.

[12] Sargent R., Verification and validation of simulation models, 16 pages. Proceedings of the 2011 Winter Simulation Conference. 2011.

[13] He Y., Makeev A., Nonlinear shear behavior and interlaminar shear strength of unidirectional polymer matrix composites: a numerical study. 11 pages. International Journal of Solids and Structures 51 (2014) 1263–1273.

Nomenclature

Symbols

A [mm^2] element cross-section area
B [mm] total width (without wrap)
E [MPa] see E_1
E_1 [MPa] element stiffness along the fibre
E_H [MPa] upper flange modulus of elasticity
E_D [MPa] lower flange modulus of elasticity
F [N] force
L [mm] element length
M [Nmm] moment
R [mm] width of the attachment
T [mm] total thickness (without wrap)
U [mm] displacement
k [mm] position along K axis
m_{TOW} [kg] is the maximum takeoff weight
t_D [mm] lower flange thickness
t_H [mm] upper flange thickness
t_O [mm] thickness of the wrap layers

α [°] characteristic angle of an element
ϵ [-] strain
σ [MPa] axial stress
τ [MPa] shear stress

Definitions, Acronyms and Abbreviations

1 primary axis of the element coordinate axis
2 secondary axis of the element coordinate axis
3 third axis of the element coordinate axis
A outer point where the landing gear is attached to the fuselage
B inner point where the landing gear is attached to the fuselage
D point, where the axle is attached to the laminate
GS Global Stiffness matrixes
GSM Global Stiffness of the whole Model
I primary axis of the element coordinate axis
J secondary axis of the element coordinate axis
K third axis of the element coordinate axis
L point, where the forces are introduced
LS Local stiffness
LSA Light sport aircraft
O wrap
T Transformation matrix
U vector of displacements
X primary axis of the global coordinate axis
Y secondary axis of the global coordinate axis
Z third axis of the global coordinate axis

2016

Modifications of a simple I-beam and its effects on the stress state

Aviation, ISSN: 1648-7788, SNIP=0.457, SJR=0.188

Volume 20, 2016 - Issue 4

MODIFICATIONS OF A SIMPLE I-BEAM AND ITS EFFECTS ON THE STRESS STATE

Jakub CEJPEK[1], **Jaroslav JURAČKA**[2]
Institute of Aerospace Engineering, Brno, Czech Republic
E-mail: cejpek@seznam.cz (corresponding author); juracka@fme.vutbr.cz

Jakub CEJPEK, Eng.
Date of birth: 1987.
Education: Eng. degree in Aeronautics, Brno University of Technology, Faculty of Mechanical Engineering, 2009 to 2011.
Affiliations: since 2011, Researcher, Brno University of Technology, Institute of Aeronautical Engineering.
Research interest: composite structures with an emphasis on thick laminates.
Publications: author of 2 conference papers.

Jaroslav JURAČKA, *Assoc. Prof. Eng. PhD.*
Education: Eng. degree in Aeronautics, Brno University of Technology, Faculty of Mechanical Engineering in1994.
PhD degree in Composite Materials, Brno University of Technology, Faculty of Mechanical Engineering in 2001.
Assoc. Prof. degree, Brno University of Technology, Faculty of Mechanical Engineering in 2005.
Affiliations and functions: 2000 to 2006, Laboratory director, Brno University of Technology, Institute of Aeronautical Engineering. Since 2005, Assoc. Prof. at Brno University of Technology, Institute of Aeronautical Engineering. Since 2012, Director of the Institute of Aeronautical Engineering at Brno University of Technology.
Research interests: composite materials, airplane airworthiness and certification.
Publications: author or co-author of 20 articles and many conference presentations.

Abstract. The motivation for this work is a desire for a deeper understanding of the structural failures in a composite glider wing, which has been tested in the laboratories of the Institute of Aerospace Engineering, Faculty of Mechanical Engineering, Brno University of Technology. To understand the causes of the encountered failures, one has to consider the effects of all the stages in the design, manufacturing and testing of the wing. This paper focuses only on the design stage. The presented facts were obtained from a finite element analysis. The geometry used for the analysis is that of the tested specimens. This allows validating the results by the comparison of the deformation and strains measured during the laboratory tests. The analysis starts with a simple I-beam loaded by three-point-bending. In the next step a cantilever is added. Several more modifications follow, changing the I-beam to the wing. The case evaluation considers the interaction between normal (material direction 1) and inter-laminar shear stresses in the upper flange. The goal of this paper is to quantify the effect of each design change in the wing structure and loading on the stress plane σ_1-τ_{31}.

Keywords: beam, normal stress, shear stress, classical laminate theory, wing, composite.

1. Introduction

The wing is the most recognizable and most interesting part of the airplane. From the design and structural point of view it seems very simple: it consists of only three different basic structural parts (beam, ribs and skin); there are no complicated mechanisms; and, most often, it is a straight and linear geometry.

In the last 110 years of aviation history and design process, a long-proven beam-theory has been used. By means of simplifications and assumptions, one can calculate the stresses in the wing and achieve a good product, which is light, yet strong enough.

The classical beam theory was created assuming a homogenous isotropic material – like steel or aluminium alloy. However, since the middle of the 20th century, a new kind of material suitable for airplane manufacturing became available on the market. This material is a composite – a combination of two different constituents. One is the fibre – giving the composite its strength. The other is the bounding agent – glue, which keeps the fibres in the right position.

Composites spread fast and many designers have found the benefits of the light-weight, sleek surface, strength, shape adjustability and good fatigue properties.

Designers and engineers used to isotropic metals had to deal with the composite anisotrophy. At first, the directional properties' difference led to a new failure

index definition. Later, the ply-nature of the composites had to be described. Thus, out of the Midlins Plate theory, the classical laminate theory has been developed (Liu 2003).

Tools dedicated to composite design evolved over the years. Most of composite design is done on a computer nowadays. However, even today, most of the computer programs still use the same assumptions about thin plates and zero through-thickness stresses. Such assumptions are not always correct and deeper analysis is required.

When discussing small airplanes, one or two seat gliders and ultralight sport airplanes, one has to keep in mind the limited possibilities of the designers in terms of technological support (material and strength tests), equipment (expensive computers and software), and, last but not least, the time pressure in the commercial environment of the companies.

These reasons left the designer with no time and/or no means for a thorough analysis. Thus, simple old analytical procedures are still used; simplifications are made. Such a rushed process forces the designers to add more layers, just to stay on the safe side. This process decreases the light-weight advantage of composite products.

The purpose of this article is to offer a new point of view towards a composite wing design method in terms of a comparison between analytical and numerical solutions of different beam shapes, ultimately evolved into a wing.

The process of a wing design will be illustrated on a real structure. The wing in question is that of a single seat, all composite glider plane, manufactured in the Kutná Hora, Czech Republic.

The results are evaluated using real laboratory tests (Juračka 2007; Matěják 2010) that took place at the Institute of Aerospace Engineering, Brno University of Technology.

2. Problem

The wing segment, which is being tested at the IAE, is of a full composite structure with thick carbon flanges. The first five tests were static tests, the next four (currently running the 9th specimen test) were fatigue tests. Tests of two whole wings were carried out as well.

The simulation and calculation is based on the wing segment, as it is smaller, and more available test data exist.

The simulated test layout is shown in Figure 1.

Fig. 1. Wing bend test

To find out where the problem of the premature failures may be, an in depth analysis of all the processes between the construction and structural design of the wing until the manufacturing is suggested.

This paper, however, focuses on the design stage only. It should answer the question as to what is the difference in the structural response of the wing segment to the introduced forces presented by analytical and numerical solutions.

This analysis will be performed on a step-evolution of the wing. It will start with a simple I-beam and finish with full wing geometry and all components of loading (Fig. 2).

To give credibility to this analysis, the finite element model shall be compared to the laboratory test.

During the laboratory tests, the failed component has been identified as the upper flange (Juračka 2007). Therefore, the analysis will focus solely on the upper flange in the root-rib area.

3. Description of the 8 steps of evolution

It has been already declared that the evolution will consist of eight steps. These step changes are to combine both, the geometry and loading schematics.

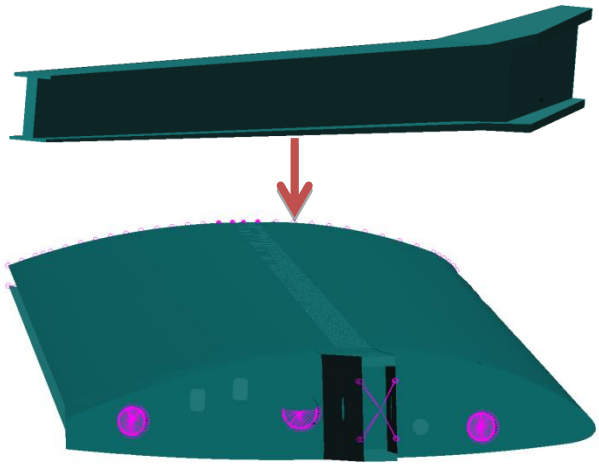

Fig. 2. Geometrical evolution: from an I-beam to a wing

The change from the I-beam to the wing will be gradual. First, the inner part of the I-beam's (*step#1*) cross-section will be replaced by a cantilever (*step#2*). Instead of one web, there will be two; the cross-section is called the "box".

The next two steps are about the transition between the cantilever and the outer wing I-beam. These changes will increase the size of the transition wall into the rib-wall (*step#3*) and rib flanges (*step#4*).

Then the rear spar and skin joins the construction (*step#5*) and helps with the load re-distribution. The final geometrical change lies in adding small stiffening ribs and making holes (*step#6*) in the root-rib (passages for the aileron and flap control mechanisms).

Further changes will take place during the loading. There will be three different loading steps, responding to the geometry change.

The first loading case (referred to as *Loading A*) is a simple three-point bending (Fig. 3) of an I-beam. This represents the fatigue laboratory test layout (Fig. 1). This loading is used for the geometrical configurations in *step#1-#6*.

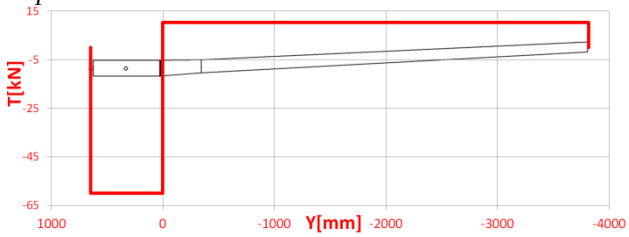

Fig. 3. Shear force distribution along the wing span, Loading A

The second loading scheme (referred to as *Loading B*) is linked to a geometry which includes the root rib and the skin with a rear spar. It will be combined with a full geometry of the wing and is called *step#7*.

The introduction of this force represents the other wing. It does not affect the flanges, at least not from the first look, but it will be investigated, because this force significantly changes the shear force distribution in the root rib. The comparison of the shear force distribution in the root rib for Loading A and B is shown in Figure 4.

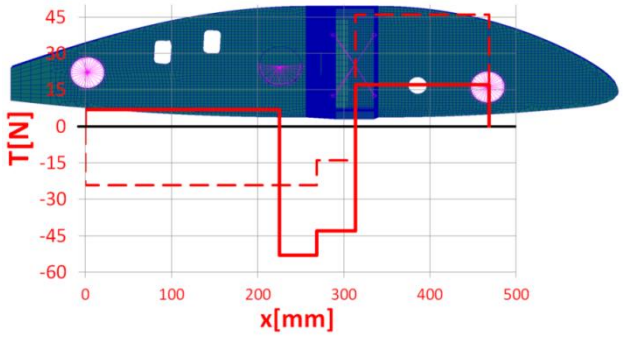

Fig. 4. Shear force distribution in the root rib: *Loading A* and *Loading B*.

Finally, *Loading C* incorporates the rest of the aerodynamical forces: the twisting moment and the longitudinal-bending force (Fig. 5).

By definition, the beam will transfer only the forces F_Z and F_X, whereas the skin will transfer the twisting moment. This assumption has been confirmed by three different finite element analyses where different combinations of forces and moments were evaluated with a resulting verdict that the twisting moment has no significant effect on the flanges or the beam itself.

In the light of this assumption the analytical calculation will not be taken into account at this moment.

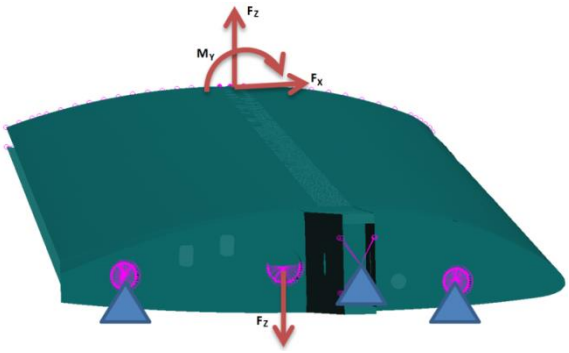

Fig. 5. Loading C

4. Analytical solution

The simple beam theory describes the stress state of a beam in terms of σ_1 and τ_{31}. The normal stress σ_1 is pure tension or compression. The shear stress along the vertical axis inside the flange is a side-effect of the principal tension/compression stress:

$$\sigma_{1(Y,Z)} = \frac{MO_{(Y)}}{J_X} \cdot Z \quad (1)$$

$$\tau_{31(Y,Z)} = \frac{T_{(Y)} \cdot S_{(Y,Z)}}{B_{(Y)} \cdot J_{X(Y)}} \quad (2)$$

However, in the business practice, the approach that is usually applied to solve the stress state is a reduced Equation 1. It is simplified to calculate the average normal stress, whereas the shear stress is thought of as non-existing:

$$\sigma_{1(Y)} = \frac{MO_{(Y)}}{H_{EF(Y)} \cdot A_{(Y)}} \quad (3)$$

The use of composite materials requires integrating all the plies into one global variable, such as E_1. Furthermore, the stresses and deformations into the individual plies need to be recalculated.

The classical laminate theory is suitable (Liu 2003) for thin-wall structures, such as the skin of the wing. One of the assumptions during the theory development is that there are only planar forces and moments acing upon the laminate plate. This assumption can be illustrated by a vector of the loading forces and moments:

$$\begin{bmatrix} N \\ M \end{bmatrix} = [N_X \quad N_Y \quad N_{XY} \quad M_X \quad M_Y \quad M_{XY}]^T \quad (4)$$

This, however, may not apply for the flanges. The flanges are by no means thin and they aren't made of plies either.

5. Numerical solution

The numerical solution, or finite element analysis, is time consuming, expensive and demanding in terms of computers, software and engineering experience.

On the other hand, the FEE offers a very detailed analysis of all 6 stress components (for solid elements) and 3 stress components for shell elements, respectively.

It provides the possibility of incorporating the adhesive contact between parts. The loading can be much more complicated.

The MSC:Patran incorporates laminate modeller software for a simple definition of the plies. But it still

uses similar assumptions as the CLT. Therefore, some important information about the stress is missing as well.

The flanges are ideal for applying solid HEX elements. This is beneficial, because it allows a direct and precise reading of the shear stress.

Another feature of the finite element analysis is the use of the contact function. This contact is a "*G*"-type, g stands for glue.

The layer of the glue that is in contact, instead of being equivalenced with the flange will significantly affect the stress in the interface.

6. Validation of the FEM

Since the laboratory tests not only provide the simple geometry and loading schematics, but also the results from the tests, it is possible to validate the finite element model against these laboratory measured parameters.

The finite element model has been validated with respect to the laboratory tests results (Matěják 2010). The validation parameters were the reaction forces, deflections and deformations. All these parameters were evaluated at 10% increments of the ultimate loading within the range from 10% to 60%.

The typical differences are provided in Table 1.

Table 1. Validation of the FEA against the laboratory test.

Condition	Difference [%]
Reaction forces	1.5–5.0
Deflection	10–15
Deformation	10

Based on these results, the FE model is declared to be trustworthy, reflecting the real construction behavior and can be used for the evolution step analysis.

7. Results of step evolution

Based on the comparison of σ_1 stress in the upper flange, especially in the root section area, the following conclusions can be formulated:

- the transition between a single and double web spar creates a large concentration of stress (approximately twice as much of σ_1 stress in the root area);
- spreading supports from within the beam to the hinge points in the rib lowers the stress by 20%;
- the flange of the rib has no significant effect on the peaks in the compression stress;
- the rear spar adds about 15% of tension stress to the root section of the flange;
- the introduction of a downward force decreases the compression stress peak at the root.

The previous Figures 6 and 7 demonstrated the relatively good agreement between the analytical and numerical solutions. Some effects that the analytical solution cannot take into account are visible, such as geometrical non-linearity.

One of the most important conditions that allows using the analytical equations states:

"The solution is valid only in a distance away of the areas of the boundary conditions." (Janíček *et al.* 1992).

That means that the analytical solution of our wing segment should not be valid, among other areas, at the root section.

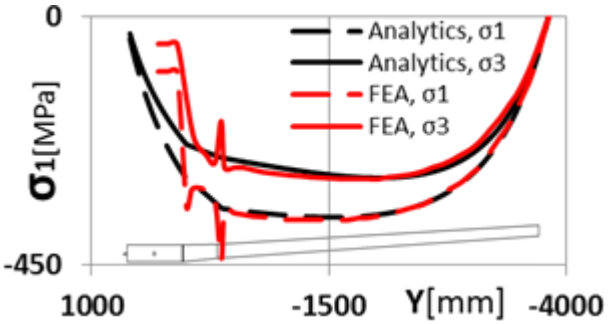

Fig. 6. Comparison of σ_1 solution, *Loading A, Step 1*.

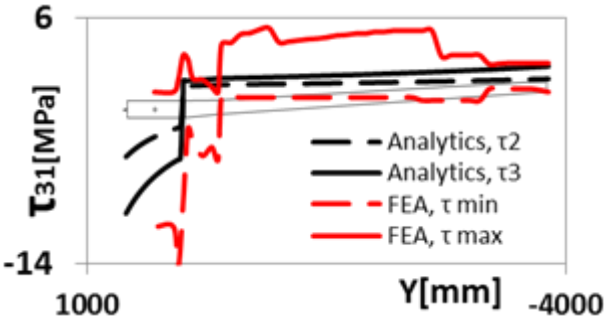

Fig. 7. Comparison of τ_{31} solution, *Loading C, Step 8*

Figure 8 shows the σ_1 stresses obtained in the root area from both solutions of the upper flange for the *Loading C*:

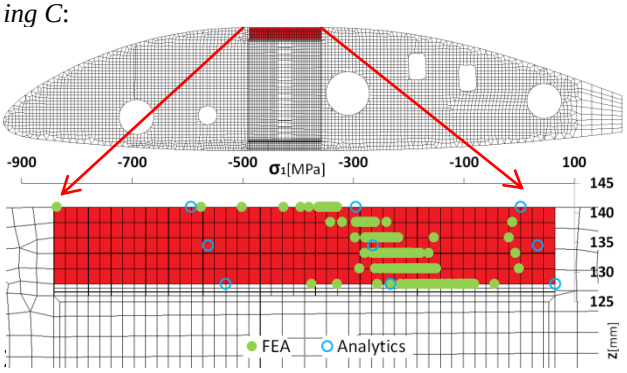

Fig. 8. Comparison of σ_1 solution, root, *Loading C, Step 8*

Figure 9 shows the influence of the web on the shear stress in the glue layer. This influence can be traces along the wing span.

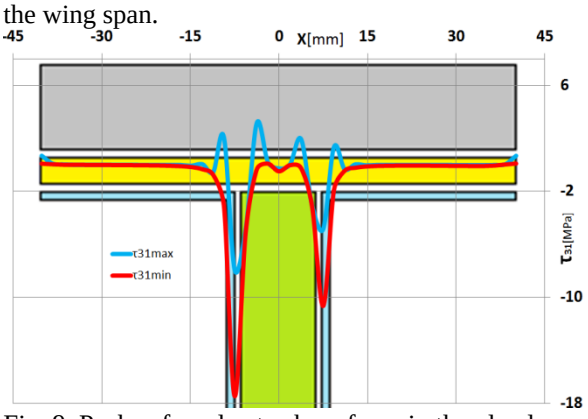

Fig. 9. Peaks of τ_{31} due to shear force in the glue layer

8. Conclusions

The step-evolution analysis has mapped the stress contribution of each geometrical change or change in the loading conditions.

Another outcome of the analysis is the comparison of the finite element analysis and the analytical solution.

The conclusion to be drawn from the method comparison is that there are significant differences, but neither is considered to be a severe overlook which might cause the failures of the structure.

The biggest impact of this in depth analysis is the definition of new questions to be answered. The questions concern the stress interaction.

The wing construction and loading strongly resemble the three-point bending tests. This obvious analogy evokes the suspicion that the elliptical failure envelope, known from the three-point bend tests, may in some way apply even here, in the wing construction, and explain the premature failures.

The shear stress τ_{31} is caused by the shear force. Focusing on the shear force distribution between the components, a distinct pattern appears in the glue layer between the web and the flange.

The peak stresses are located in the positions of the glass-fibre walls of the web.

Dedication

These outputs were supported by the project KhAI-ERA – Integrating the National Aerospace University KhAI-ERA into ERA (FP7-INCO-2011-6) with the cooperation of NETME Centre, regional R&D centre built with the financial support from the Operational Programme Research and Development for Innovations within the project NETME Centre (New Technologies for Mechanical Engineering), Reg. No. CZ.1.05/2.1.00/01.0002.

References

Juračka, J. 2007. *Referenční statická zkouška segmentu křídla*. IAE report. 34 p.

Janíček, P.; Ondráček, E.; Vrbka, J. 1992. *Pružnost a pevnost I*. VUT v Brně.

Liu, Y. 2003. *Introduction to the finite element method*. CAE Research Laboratory. 188 p.

Matěják, V. 2010. *Laboratory strength test methodology of 304s wing*. IAE report. 13 p.

2015

Acoustic Emission Localization in Testing of Composite Structures

Applied Mechanics and Materials, ISSN: 1662-7482

Volume 821, 2016

Applied Mechanics and Materials Vol. 821 (2016) pp 405-411
© (2016) Trans Tech Publications, Switzerland
doi:10.4028/www.scientific.net/AMM.821.405

Submitted: 2015-06-12
Revised: 2015-08-26
Accepted: 2015-08-26

Acoustic Emission Localization in Testing of Composite Structures

WEIS Martin [1a], CEJPEK Jakub[1b] and JURAČKA Jaroslav[1c]

[1]Institute of Aerospace Engineering, Faculty of Mechanical Engineering, Brno University of Technology, Czech Republic

[a*] weis@fme.vutbr.cz, [b] y100957@stud.fme.vutbr.cz, [c] juracka@fme.vutbr.cz

Keywords: Acoustic emission localization, non-destructive testing, monitoring, acoustic emission detection.

Abstract. Acoustic emission (AE) is current trend of non-destructive monitoring methods. It suits perfectly for supporting of fatigue tests. The method is also applicable in monitoring of quasi-static tests. AE helps the engineers to understand the degradation process in the tested object and also keep track of the failures. This article offers an insight into the practical experience with acoustic emission. Tests of three different composite structures (wing, fuselage and hull panel) were chosen to illustrate the application of AE monitoring system during fatigue and quasi-static tests. These tests have shown that accuracy of localization is sufficient to identify damaged areas. Moreover, the system may offer an early warning of upcoming failure.

Introduction

Passive acoustic emission detection has been used at the Institute of Aeronautical Engineering (IAE) for almost a decade. This method is non-destructive monitoring tool used for keeping track of structural failures in the specimen during laboratory test. Passive means, that the sensors, attached to the tested specimen are only *"listening"* to the emissions produced (emitted) by component due to the introduction of external loading. Detected acoustic emission signal has commonly a character of an ultra-sound frequency. The released energy travels through the structure with certain speed, specific to each material.

There are two types of localization: linear (Fig. 1a) and planar (Fig. 1b). Linear localization does not demand as many sensors as planar; therefore it allows the user to investigate larger specimens, such as the wing. Employing fewer sensors is an advantage in fatigue tests because of lower memory storage requirements. This sensor layout allows identifying problematic areas.

On the other hand, planar localization provides more accurate location of the emission source. It has been applied in later stages of fatigue test.

As for quasi-static tests, planar localization is more suitable as the test does not provide the time to identify the problematic area. For identifying the problematic areas one has to use either the Finite Element Analysis (FEM) or educated guess.

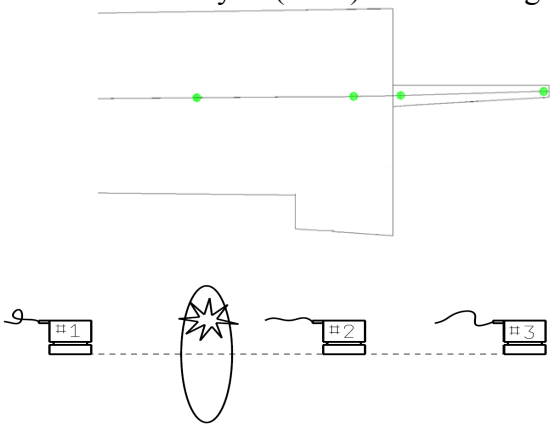

Figure 1a: Linear localization.

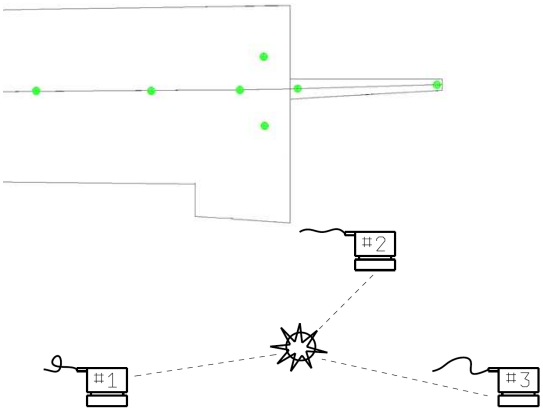

Figure 1b: Planar localization.

Figures 1a and 1b show the layout of the sensors (green points) on the wing segment during fatigue test. There is also an illustration of geometrical precision (planar is more accurate).

Very important aspect of the method is the physical accuracy of localization. Prior each test a calibration procedure has to be completed in order to establish the emission propagation velocity between each pair of sensors.

Each sensor has an interval of signal frequency which it is able to detect. In case of global localization, hi-frequency sensors (100-300kHz) are used in order to cancel out the noise. For detailed analysis of extremely loaded area, low-frequency sensors are used (30-60kHz) [1].

Example of determining the speed of acoustic signal propagation follows:

Tested specimen is a composite wing with carbon fibre flanges. Flanges are the primary area of interest and they will be monitored by linear localization sensor setting.

A pen-test (as described in [2]) between two sensors is conducted and evaluated. Measured velocity of propagation is 8000m/s. Moreover, pen-test allowed establishing the accuracy of the method. The error of localization turned out to be less than 10mm (Fig. 2). This procedure used program *"Deamon"* [3].

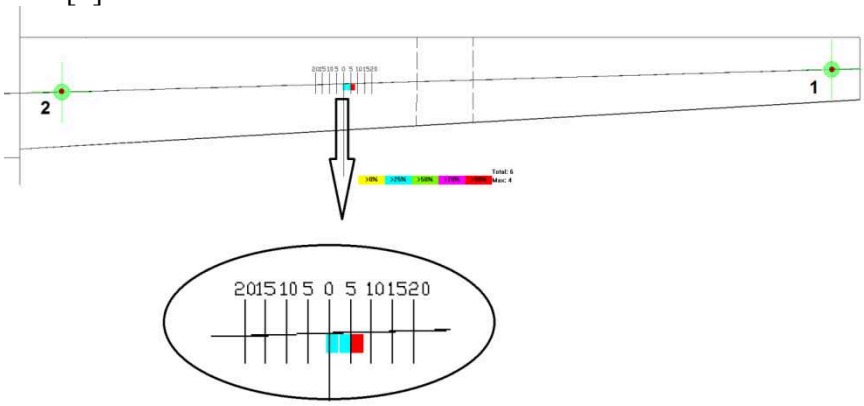

Figure 2: Pen-test and accuracy of the localization.

Quasi-static Strength Test of VUT-061 Fuselage

VUT-061 is in-house designed and built light two-seat aircraft. A strength test of the fuselage has been planned as a part of the air worthiness proceedings. At first a finite element analysis has been used to simulate the structural response and to predict the problematic areas. According to this prediction a bunch of sensors was placed around the critical area and then the strength test started.

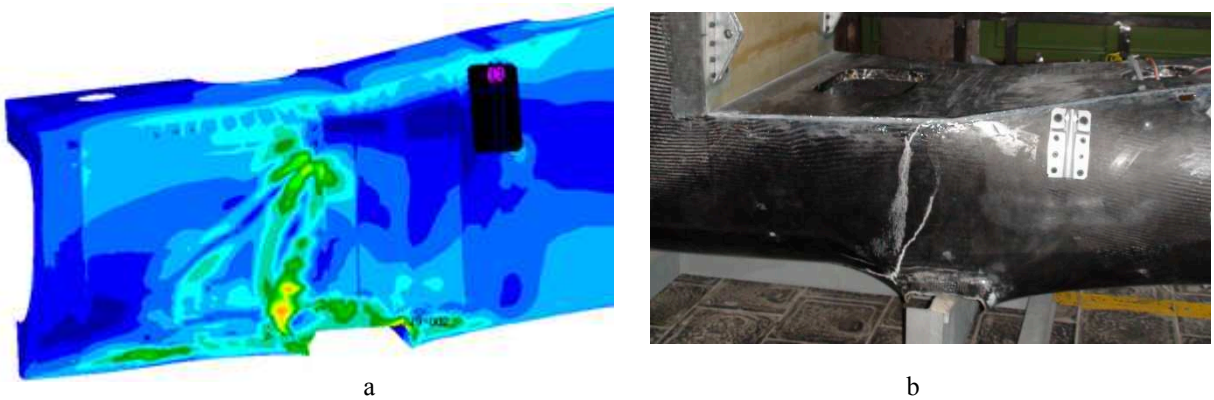

a b

Figure 3a,b: FEM simulation (a) predicted critical area, strength test until destruction (b). [4]

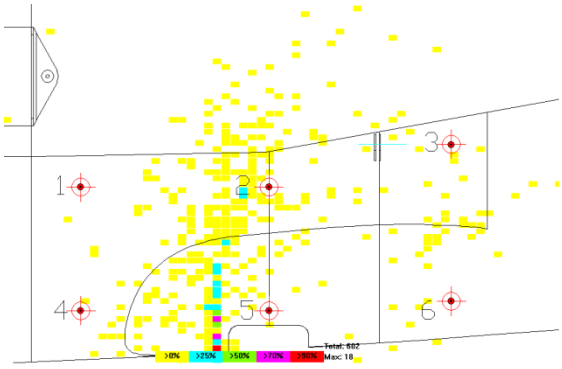

Figure 3c: Acoustic localization of the failure location. [4]

Figures 3a-c show a perfect correlation between the theory (simulation) and real laboratory test. Still, this is not where the post analysis of acoustic emission ends. The thorough post-analysis has shown the difference between failure of the foam core (crushing) and skin failure.

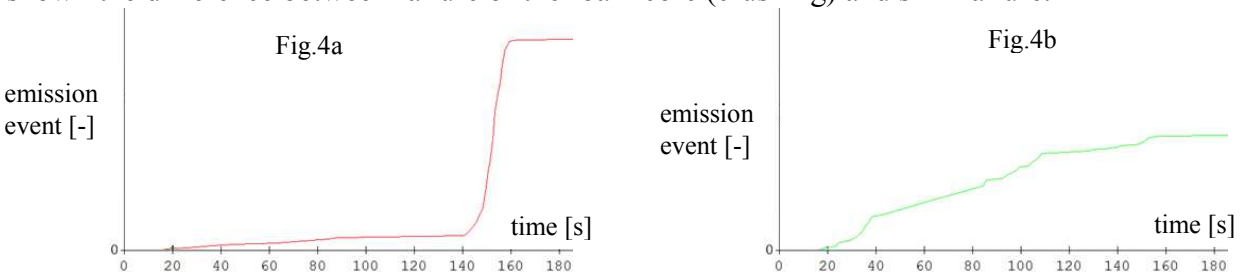

Figure 4: Post analysis of skin failure (a) and core crushing (b).

From certain load level the foam core starts to be crushed (Fig. 4b, time 20s). This crushing emits sound waves that are detected by all sensors around the damaged area. The vertical axis show cumulative number of emission events.

Fast failure of the skin is shown with red curve (Fig. 4a). This was obtained from reduced number of sensors near to the failure itself. Skin has failed at time around 150s.

Quasi-static Test of CRP Composite Panel

Tested carbon panel consists of skin, bulkheads and stringers. Loading is quasi-static compression. A total of 10 sensors were placed on the skin surface, as shown in Fig. 5, and the loading started.

A sudden structural failure occurred quickly and without prior warning. Acoustic analysis of this test registered only a few emission events.

Small amount of data recorded and fast destruction did provide no reasonable data to make conclusions as to where and when the failure was initiated.

Also it has been discovered that the sensors are prone to falling off at the time of destruction.

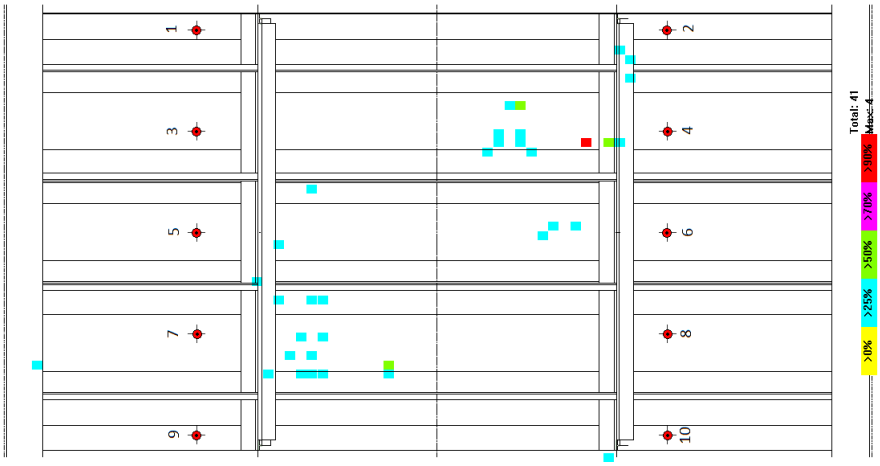

Figure 5: Carbon composite panel offered only a few emission events to analyse.

Fatigue Test of Composite Wing Segment

The acoustic emission is easily applicable on the composite wing under fatigue test. AE offers quite accurate structural-health monitoring. The drawbacks are mostly in the need for experienced personnel and – in case of long fatigue tests – huge data storage and computer processing capacity.

A series of wings and wing segments were tested (under both quasi-static and fatigue loading) [5] at the IAE. The series of four wing segment fatigue tests were preceded by series of 5 quasi-static tests as part of airworthiness certification (first in 2004). First fatigue test (specimen #6) was running in period from September 2007 till April 2008. As it was the first fatigue test of its kind at the institution, all parameters had to be defined and the experience had to be gained. After other two segments were tested, changes in design were made and sample #8 has been tested under quasi-static loading in February 2010 (sample #8 was a full scale wing). AE has been involved in this static test; however the results were inconclusive because the failure occurred at different area than predicted.

Similar test of beam segment of wind turbine blade has been conducted in Germany [6]. The test aimed to analyse the shear glue bound of the flanges and the web.

Since January 2013 until August 2014, wing segment #9 has been tested. This test will be discussed further in this article.

Strategy for monitoring of segment #9 was to employ linear localization at the beginning of the test. Normally this would be due to initial analysis of potential problematic area. Since this segment was the 9th of its kind and problematic areas were known, this precaution served to minimize the amount of data generated by the monitoring. When the number of emission events started to rise more sensors were added in order to have the advantage of planar localization.

More than global structural failure of the whole segment the acoustic emission localization has discovered local problems – such as steel pin failure or layup delamination.

The root rib is connected by two steel pins to the fuselage (during the test the fuselage is replaced by a device introducing the correct loading of the wing.

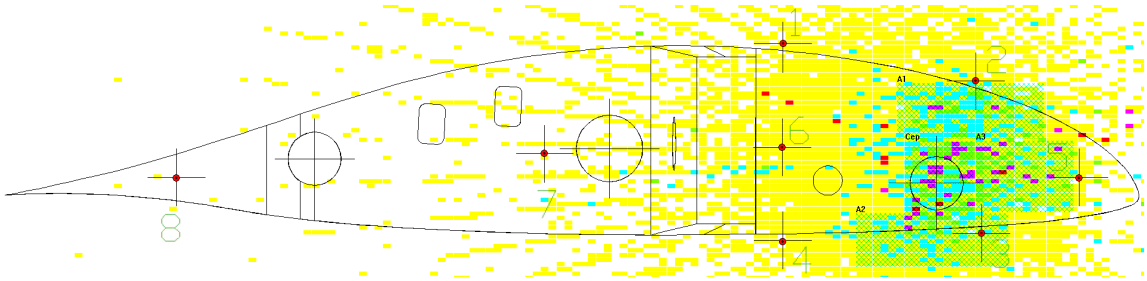

Figure 6: Root rib pin initiates emissions.

Monitoring system has discovered, that in the area of the leading edge pin there is located a problem (Fig. 6). However it is the engineer who must figure out what is the cause for increased acoustic activity. It may be separation of composite rib and the steel housing of the pin. Other possibility is the pin itself (Fig. 7).

Figure 7: Root rib pin has failed. After it has been repaired, the fatigue test continued.

Increased activity has been indicated on the web. After the examination a delamination has been discovered (Fig. 8) in the area where the carbon part of the web ends. This delamination can be a result of the loading or it could have been created during the manufacturing.

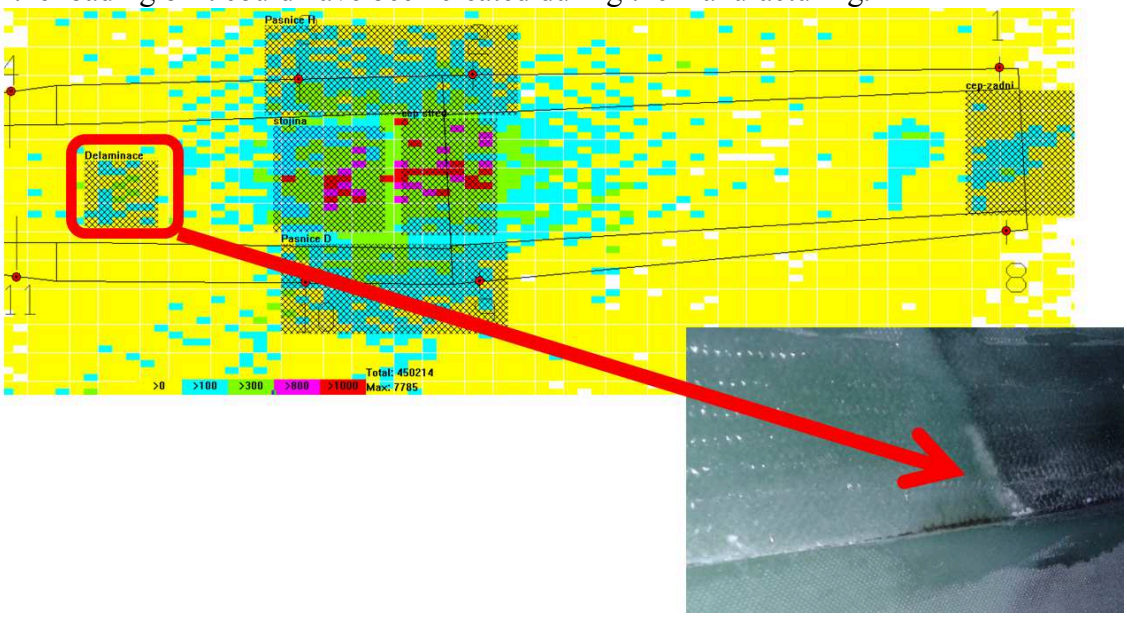

Figure 8: Delamination on the web.

Recognising of certain types of failures can be achieved through an analysis of the types of the signal. Ono and Gallego summarized [7] the types of failure in composite and paired it with typical frequencies of the acoustic emission caused by these failure. For example delamination induced signals in cross-ply glass fibre composites, such as the case described above, are emitted on frequencies under 400kHz.

Probably the most interesting failure is the last one that ended the fatigue test. Huge concentration of acoustic emission spiked during weekly check in the area of the cantilever pin (position 1-8 on Fig. 9). However, this spike disappeared when evaluating longer period (Fig. 10).

Based on the evaluation of longer period (Fig. 10) it has been decided to neglect the rising emission event number in the cantilever pin.

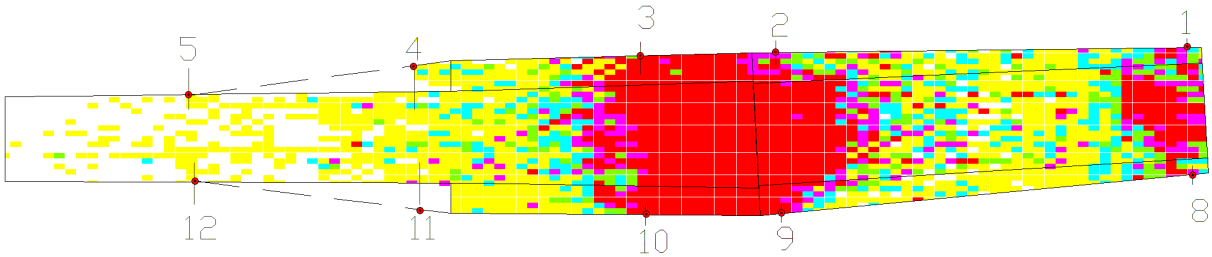

Figure 9: 12% of life #4, all sensors (weekly inspection).

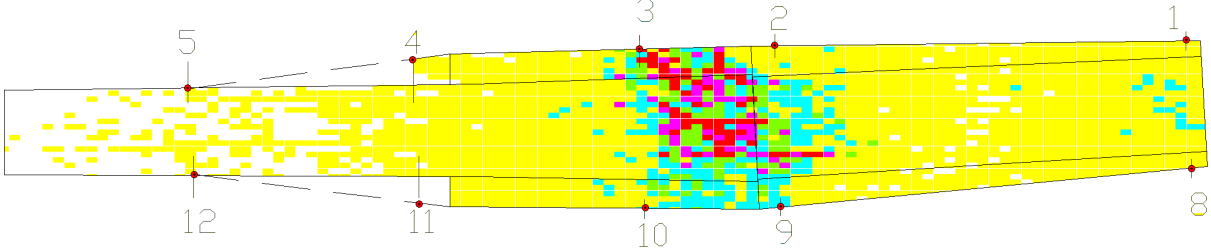

Figure 10: 100% of life #4, all sensors (whole life cycle number 4 evaluated).

Therefore the fatigue test continued for few more days. Then the cantilever pin failed (Fig. 11).

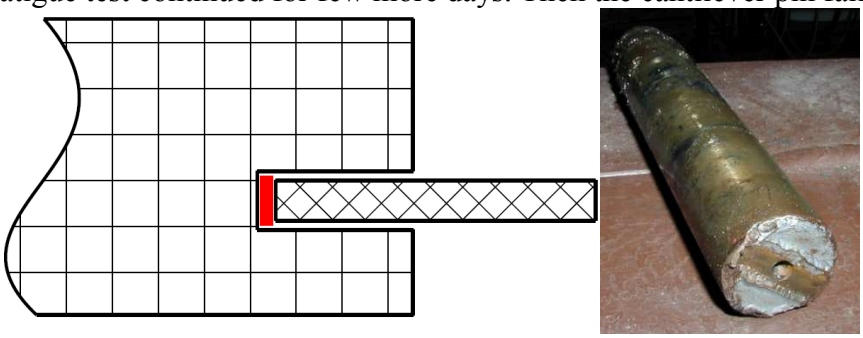

Figure 11: Cantilever pin has failed in the place, where it was welded.

What happened was that the evaluation of the whole life #4 cycle has disguised the spike in the critical area, there was no direct personal check of this pin (because it would require complete disassembling of the set). The failure of the cantilever pin has subsequently led to a critical damage of the web and to the end of this fatigue test.

Conclusions

The passive acoustic emission analysis is a very good non-destructive method of problem localization. In combination with the composite materials the most successful usage is during the long-duration fatigue tests. Also very successful application is quasi-static monitoring of slow-failing structures.

Practical experience with AE localization on composite structures is very positive. It allows to monitor the fatigue tests and to discover potential problem. Knowledge of position of where the problems are allows the personnel to stop the test and identify exactly the nature of the problem and to take actions.

In case of quasi-static tests, the post processing can distinguish between different types of failures (core crushing and skin failure).

Summary of the practical experience with the AE localization:

Advantages:

+ good accuracy of localization,
+ different application: fatigue and quasi-static tests,
+ sample or full size product monitoring.

Drawbacks:

– difficult to recognize the source (pin, bearing, delamination…),
– need for large data storage and processing capacity.

Where to use AE localization analysis?

- long fatigue tests,
- appropriate structures under quasi-static loading.

How to use AE analysis during fatigue tests?

- weekly evaluations,
- monthly evaluation,
- after-period evaluation.

Acknowledgement

These results were supported by the project TE02000032 - Advanced Aerostructures Research Centre. This project was realized with financial support from national budget of the Technology Agency of the Czech Republic.

References

[1] Standard ČSN EN 15857 Non-destructive testing - Acoustic emission. Czech Office for Standards, Metrology and Testing, 2010 (in Czech).

[2] Přibáň, M., Acoustic emission (AE) – theory and practice, VUT Brno, 2012

[3] Dakel, XEDO-Daemon: User manual, 2008

[4] Vaněk, F, Strength test of VUT-061 Turbo fuselage - PZ83, Brno University of Technology, 2012

[5] Juračka, J.; Weis, M., Augustin, P., Fatigue Test Progress of 304 S Wing Segment, Brno University of Technology, 2014

[6] Weihnacht, B., Schulze, E., Frankenstein, B., Acoustic Emission Analysis in the Dynamic Fatigue Testing of Fiber Composite Components, 31st Conference of the European Working Group on Acoustic Emission

[7] Ono, K., Gallego, A., Reasearch and Application of AE on Advanced Composites, Journal of Acoustic Emission, volume 30, pages 180-220, 2012

2013

Napěťově-deformační analýza segmentu kompozitového křídla

Příspěvek na konferenci „Setkání uživatelů MSC.Software s.r.o. 2013“

Setkání uživatelů MSC.Software s.r.o. 2013. ISBN: 978-80-260-4173- 3.

Napěťově-deformační analýza segmentu kompozitového křídla

Ing. Jakub Cejpek

16. května 2013

e-mail: y100957@stud.fme.vutbr.cz

Letecký ústav, Fakulta strojního inženýrství, Vysoké učení technické v Brně

Abstrakt

Předkládaný článek obsahuje popis přípravy a průběh konečnoprvkové pevnostní analýzy segmentu kompozitového křídla pomocí programů Patran Nastran. Simulovaná geometrie i zatížení odpovídají reálné předloze, zkoušené na Leteckém ústavu. Simulované varianty obsahují různé druhy elementů a okrajových podmínek. Výsledky jsou porovnány s analytickým výpočtem.

Článek obsahuje výčet některých nedostatků metodiky návrhu kompozitních křídel. Pokouší se na tyto nedostatky upozornit díky poznatkům získaných z provedených simulací. Celá simulace, stejně jako pevnostní zkoušky, se soustředí na kořenovou část křídla. Tomu je uzpůsobené definované zatížení jež vyvozuje reálný napjatostní stav právě ve zkoumané kořenové oblasti.

1 Úvod

Návrh kompozitních křídel pro kluzáky byl po dlouhou dobu řešen tradičními zažitými metodami. Tato metoda zanedbává některé významné faktory, jako například:

- velké deformace křídla,
- rozdílnost závěsů křídla,
- dopředná složka zatížení,
- velká štíhlost.

Tato neadekvátní metoda se projevila během pevnostních zkoušek nižší únosností a životností, než bylo původně predikováno [1]. Použití zjednodušené metodiky, zanedbávající podstatné vlivy, bylo způsobeno absencí prostředků (výpočetní výkon a software) pro detailnější analýzu složitých konstrukčních celků. Nyní však nastala možnost i potřeba detailnější analýzu provést, a to přímo se znalostí výsledků zkoušek reálné konstrukce.

Pro konečnoprvkou analýzu je použit Nastran. Příprava vstupního souboru do Nastranu byla provedena v programech CATIA a Patran, přičemž silným pomocníkem při této analýze je modul laminate modeler, který umožňuje vytvářet korektní vrstvení na značně zakřivených plochách.

Geometrie zkoušených segmentů byla přenesena do počítače, doplněna o geometrii od výrobce [2] a byla zahájena příprava detailní konečno-prvkové analýzy.

2 Příprava analýzy

2.1 Geometrie

Z geometrického hlediska se křídlo dělí na nosnou plochu (délka 3,8m) a krakorec (o délce 604mm).

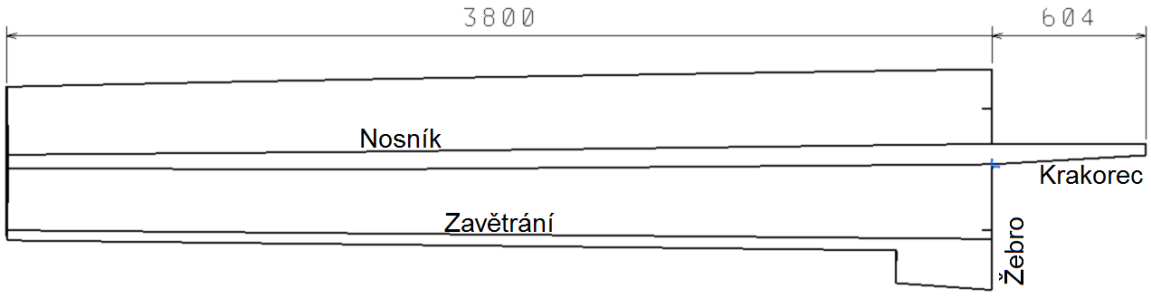

Obrázek 1: Půdorys segmentu křídla. Nosná plocha o délce 3800mm a krakorec o délce 604mm.

Z konstrukčního hlediska jde o jednonosníkovou konstrukci s nosným potahem a zadním zesíleným zavětráním. Spojení křídel a trupu je řešeno následovně:

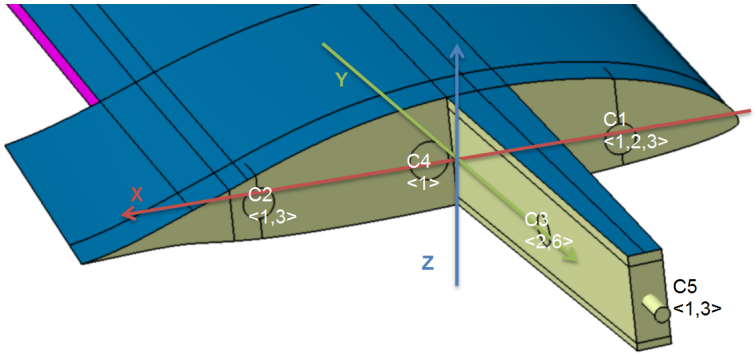

Obrázek 2: Polohy závěsů křídla: C1 a C2 přední a zadní čep; C3 spojovací čep křídel; C4 ložisko pro palec pravého křídla, C5 palec. Čísla v ostrých závorkách korespondují s okrjaovými podmínkami zadávanými v Patranu.

Přední a zadní čepy přenášejí pouze translační sílu (rovina XZ a směrem +Y). Čep C3 slouží ke spojení obou polovin křídla tak, aby se nevysunuly. Kloubové ložisko C4 a čep C5 slouží k přenosu ohybového momentu mezi křídly. Pravá a levá polovina křídla nejsou symetrické kvůli principu závěsů C4 a C5. Levý nosník uhýbá dopředu, pravý dozadu.

Kvůli symetrii zatížení by mělo platit, že vertikální síla v ložisku C4 a palci C5 jsou téměř totožné.

2.2 Materiál a skladba

Materálové charakteristiky jsou dobře známy, všechny použité materiály byly měřeny na LÚ.

Skladba vrstev je uvedena v [1]. Například schéma vrstvení kořenového žebra vypadá následovně:

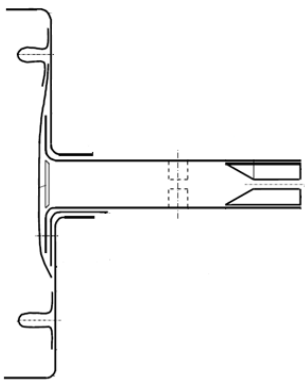

Obrázek 3: Půdorysný řez kořenovým žebrem a krakorcem znázorňující styl vrstvení.

2.3 Zatížení a okrajové podmínky

Pro simulaci byly zvoleny okrjaové podmínky z reálného letadla a silové a momentové zatížení odpovídající zkoušce. Vetknutí simuluje reálný stav za letu, tedy že čepy C1 a C2 přenáší posouvající sílu do trupu, palec C5 s ložiskem C4 ohybový moment mezi křídly a čep C3 zabraňuje vytažení křídel z trupu a též se podílí na přenosu ohybového momentu.

Za povšimnutí stojí funkce čepů C1 a C2 co se týče posuvu v ose Y. Toto spojení je realizováno pomocí trupových čepů opřených do ložisek v žebru. Způsobem, jakým je křídlo zatíženo, dochází k tlaku do čepu C1 směrem do trupu a vytahování ložiska z čepu C2 směrem ven z letounu.

Aerodynamické silové zatížení je pro potřebu zkoušky kondenzováno do tří složek (síly do směru Z a X a momentu ve směru Y) působící na konci segmentu. Toto zjednodušení způsobuje to, že reálný napjatostní stav nastává pouze v oblasti kořenového žebra. Protože k poruchám během fyzických zkoušek dochází právě v tomto místě, je toto zjednodušení akceptovatelné a simulace má pro tuto oblast svou výpovědní hodnotu.

Jako náhrada pravého křídla je do ložiska C4 zavedena síla, která je iterativně naladěna se silovou reakcí v čepu C5.

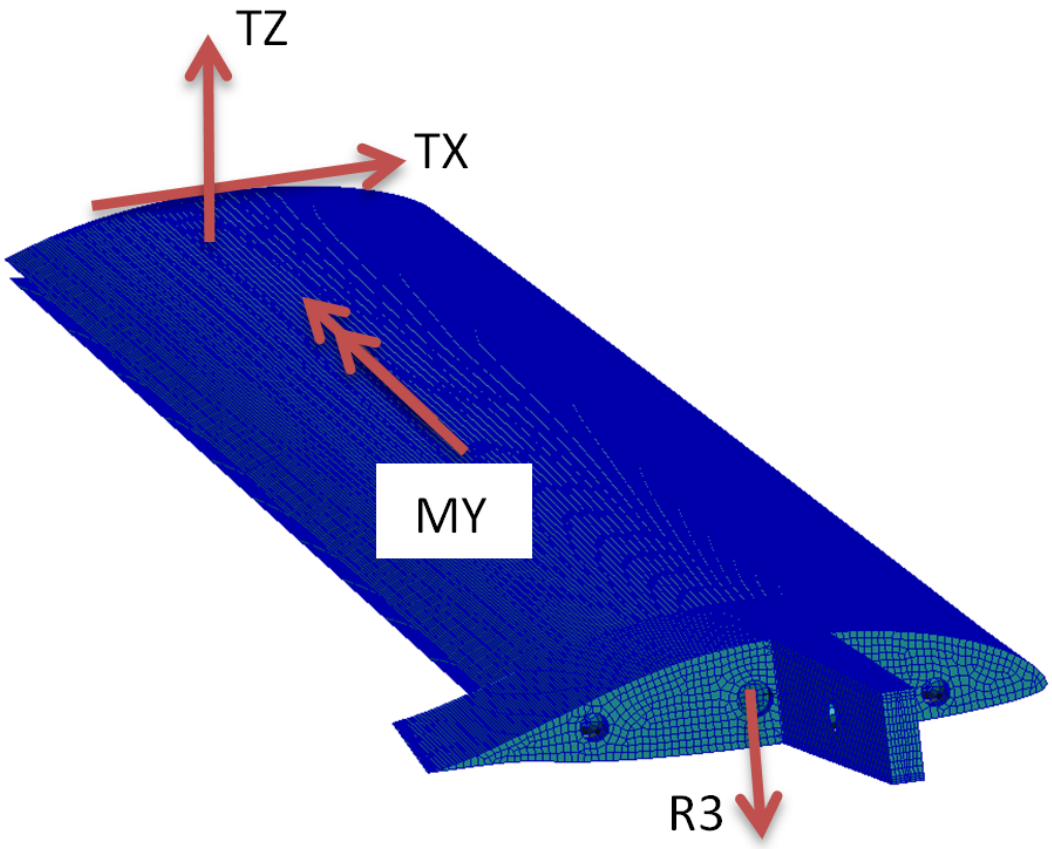

Obrázek 4: Kondenzované zatížení segmentu křídla.

2.4 Analytický výpočet

Pro potřeby hodnocení konvergence simulací byl proveden orientační analytický výpočet statické rovnováhy a rozložení extrémů napětí po rozpětí segmentu křídla.

Statická rovnováha a reakce ve vertikálním směru (osa Z) byly spočteny pro kontrolu reakcí ve vetknutí a rychlejší získání síly R3 během výpočtů.

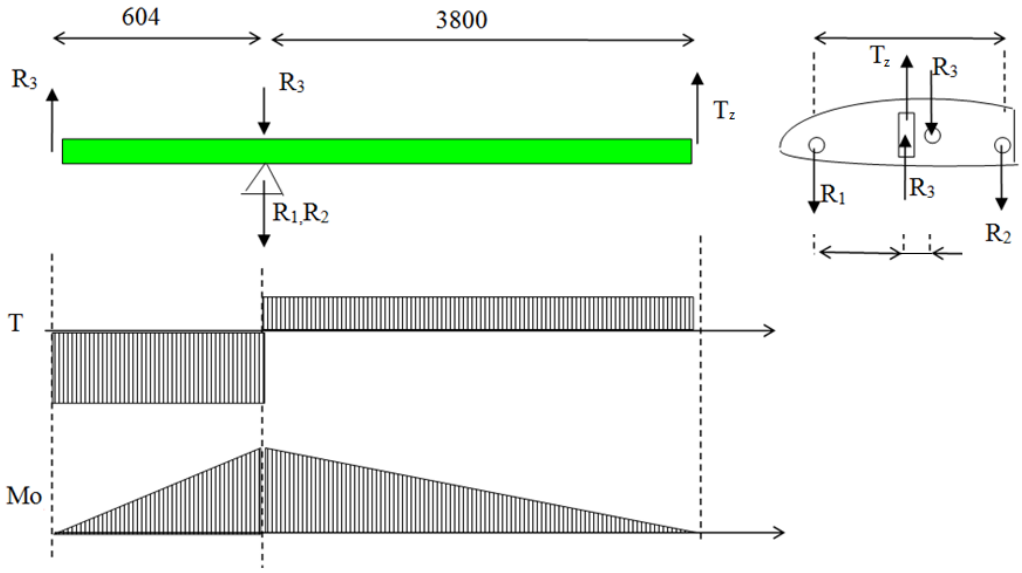

Obrázek 5: Silová rovnováha křídla.

Jako kontrolní hodnoty byly spočteny průběhy napětí po rozpětí. Pro zjednodušení byl segment křídla zredukován pouze na vetknutý nosník (vetknutí v kořenovém žebru) a ten je zatížen silami TX a TZ. Toto zjednodušení je aplikovatelné, protože zatížení od momentové složky MY je zanedbatelné. Malý význam zatížení od MY potvrdil i porovnávací výpočet v Nastranu. Extrémy napětí od kombinovaného namáhání byly identifikovány následně:

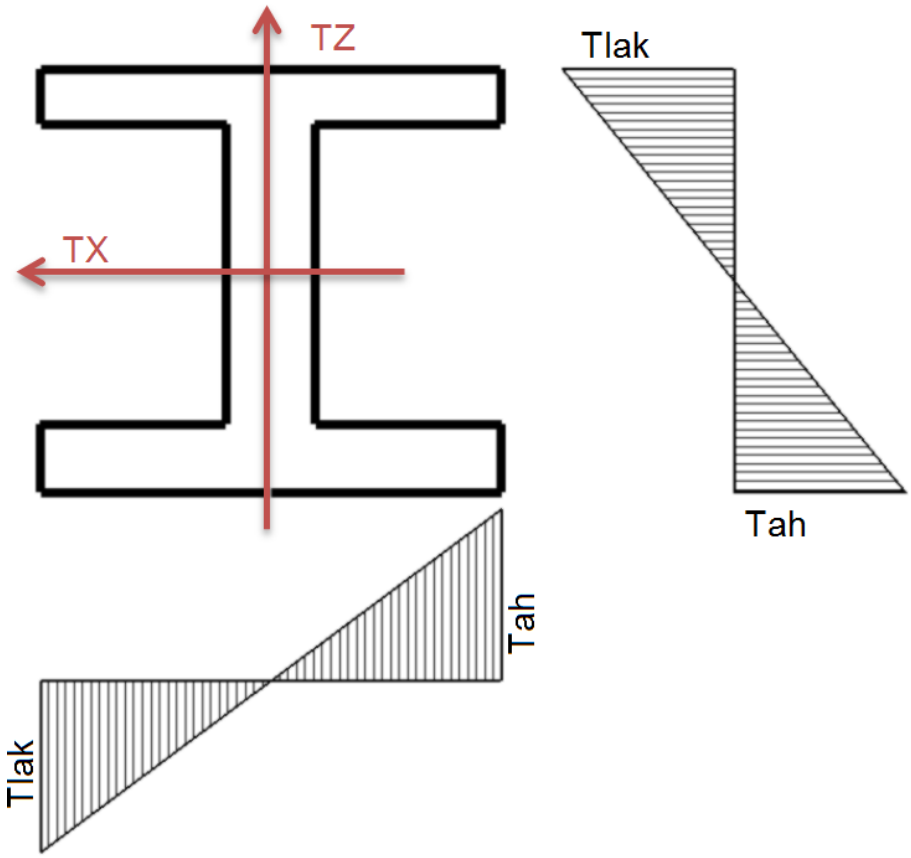

Obrázek 6: Polohy extrémů napětí na příčném řezu nosníku.

- Ohyb od síly TZ: horní pásnice tlačená, dolní pásnice tažená,

- ohyb od síly TX: přední části pásnic tlačené, zadní vlákna tažená.

Touto analýzou byla stanovena kritická místa pásnice: maximální tlak je v horní pásnici na předním vláknu, zatímco maximální tah je v dolní pásnici na zadním vláknu.

3 Modelování

Pro všechny publikované výsledky byl použit řešič SOL106 s deseti kroky řešení a výstupním souborem OP2. Výsledná napětí jsou uváděna jako halvní napětí ve vlákně (σ_X).

3.1 Vrstvení

Kvůli komplexnímu charakteru vrstvení byl model rozdělen do 4 skupin s vlastními laminate modeler LM-soubory:

- horní potah,
- dolní potah,
- stojiny,
- žebra.

Každá skupina obsahuje různé podskupiny obsahující elementy na ploše korespondující s určitou laminou a materiálem. Jako první vznikla příručka popisující jednotlivé vrstvy (oblast modelu, materiál, orientace). Například zesílené kořenového žebra na dolním potahu obsahuje 8 vrstev z materiálu označeného MAT5 pod úhlem 45° od předem stanoveného směru. Celá vrstva (ply) se jmenuje LMgrupDolni_#4d:

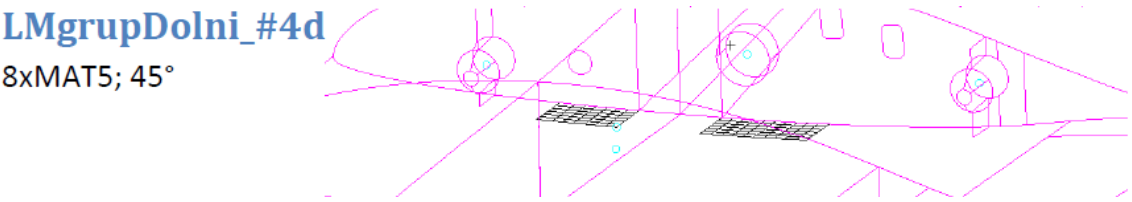

Obrázek 7: Příklad definice vrstvy. Vyznačené elementy patří do skupiny dolního potahu s číslem 4d. Vrstvení je z materiálu MAT5 pod úhlem 45°. Celkový počet vrstev je 8.

V dalším kroku byla sestavena tabulka se sekvencí a počtem vrstev:

Vrstvení skupiny LMgrup_Zebro

Referenční směr: globální osa X, případně Y

Grupa #	Materiál	Orientace	Počet vrstev
1	5	45	16
2b	5	45	6
2c	5	45	6
3	5	45	10
2a	5	45	5
2d	5	45	5
4	5	45	5
5	5	45	5
6	5	45	17
2e	5	45	6
7	5	45	4
8	5	45	8
9	ocel	0	3mm

Obrázek 8: Sekvence vrstev žebra.

Tato sekvence vrstev byla zadána do Lay-Up souboru. Pro snazší orientaci v post-processingu byly rozlišeny čísla vrstev a názvy skupiny. Počátek sekvence pro horní potah vypadá takto:

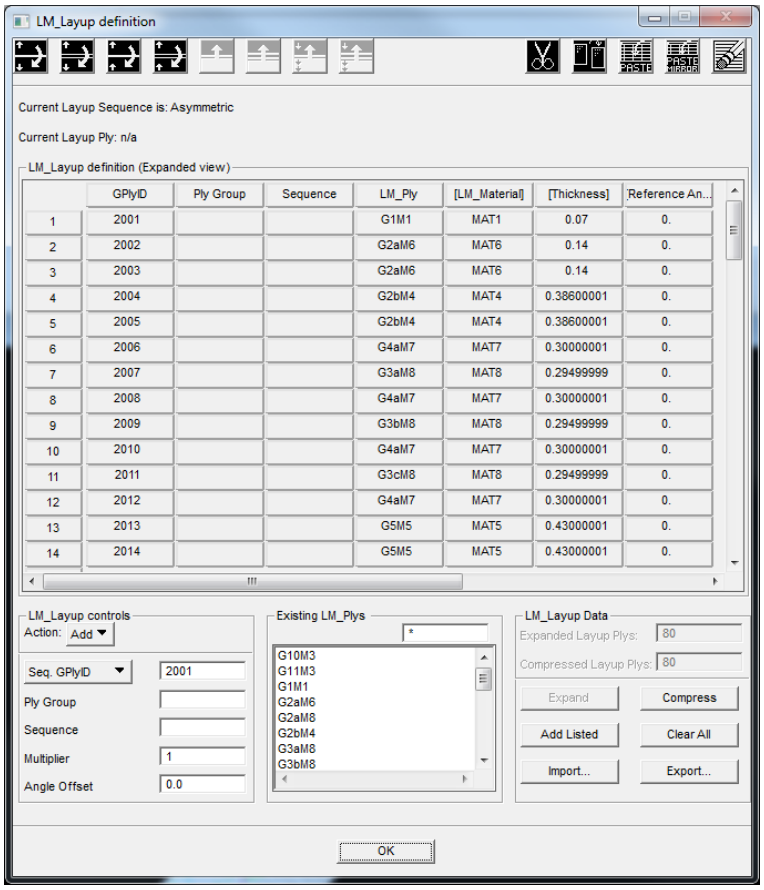

Obrázek 9: Část Layup tabulky pro horní potah.

3.2 2D model

Jako první model vznikla pouze jednoduchá 2D síť s proměnnou hustotou elementů. Od konce segmentu se síť zhušťuje směrem ke kořeni. Použité elementy jsou pouze lineární QUAD a TRIA. Pro zavedení okrajových podmínek byly použity MPC prvky typu RBE2.

Počet nodů: 13414

Počet elementů: 13860

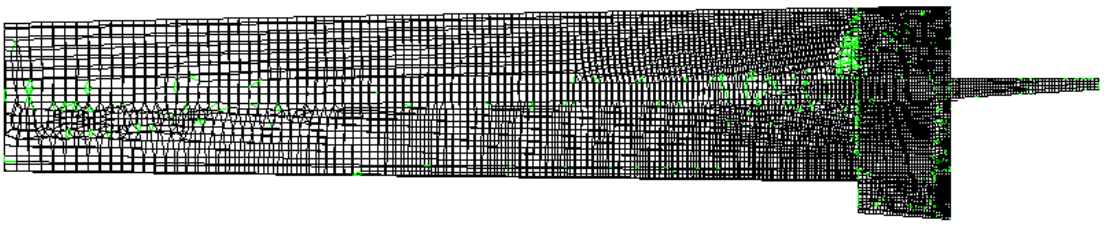

Obrázek 10: Půdorys křídla s 2D meshí.

3.3 3D model

Pro detailnější analýzu byl model upraven a pásnice, lepidlo a stojina byly modelovány pomocí 3D elementů. Tato síť má téměř konstantní velikost elementů po celé délce. Zavedení okrajových podmínek je identické s 2D modelem.

Počet nodů: 112908

Počet elementů: 121739

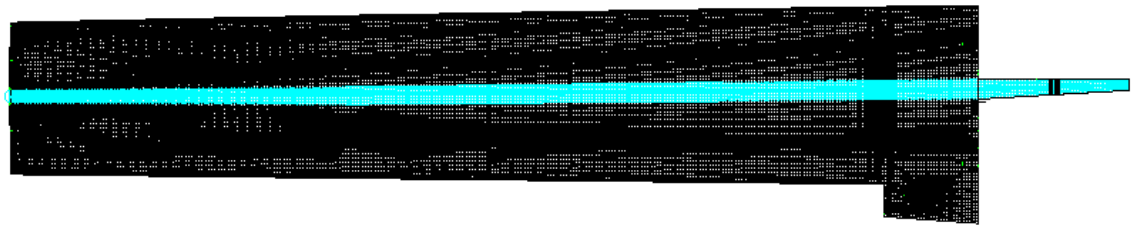

Obrázek 11: Půdorys křídla s 3D meshí.

Hlavní rozdíl oproti čistě plošné síti jsou objemové elementy ve stojině a pásnicích. Též přibyla vrstva 3D elementů reprezentující lepidlo:

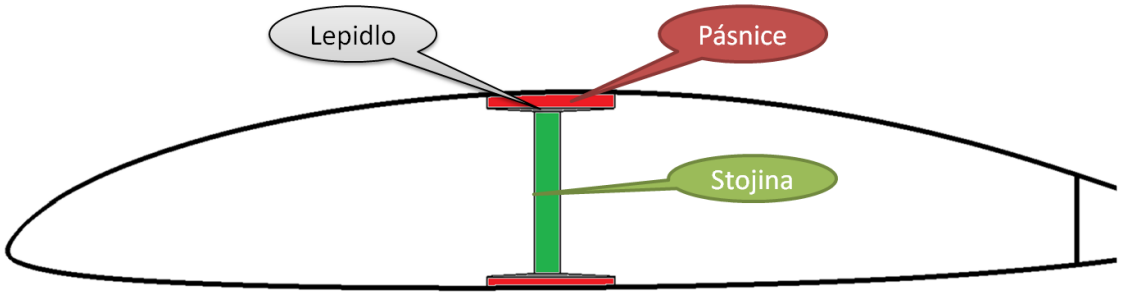

Obrázek 12: Řez křídlem znázorňující rozložení 2D elementů a 3D elementů (lepidlo, pásnice, stojina).

Pro pásnice byl použit 3D ortotropní materál, stojina a lepidlo jsou modelovány jako bilineární isotropní materiál.

3.4 Výsledky a porovnání modelů

Iterační metodou byly nastaveny okrajové podmínky (síla R3 do žebra, vetknutí). Výsledný model byl spočten nelineárním řešičem SOL106 a porovnán s analytickým výpočtem. Následující grafy znázorňují extrémy napětí v pásnicích po délce rozpětí segmentu křídla.

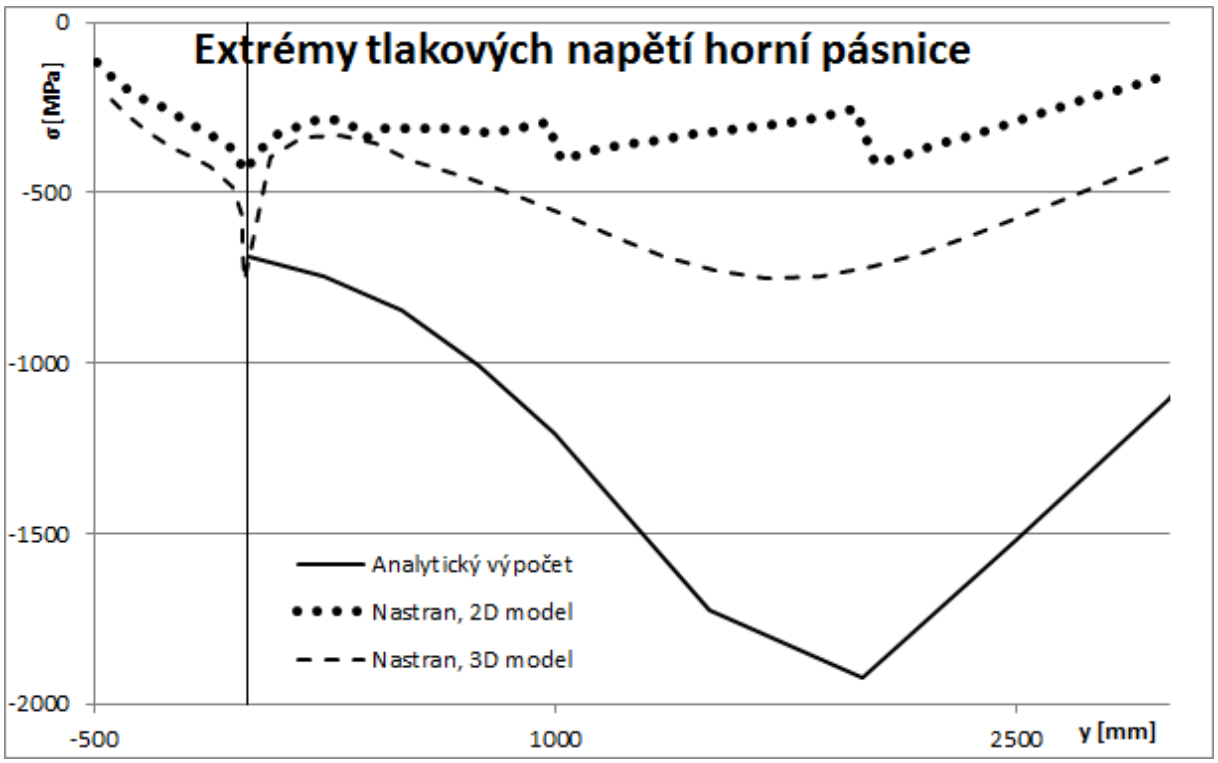

Graf 1: Průběh tlakových napětí horní pásnice.

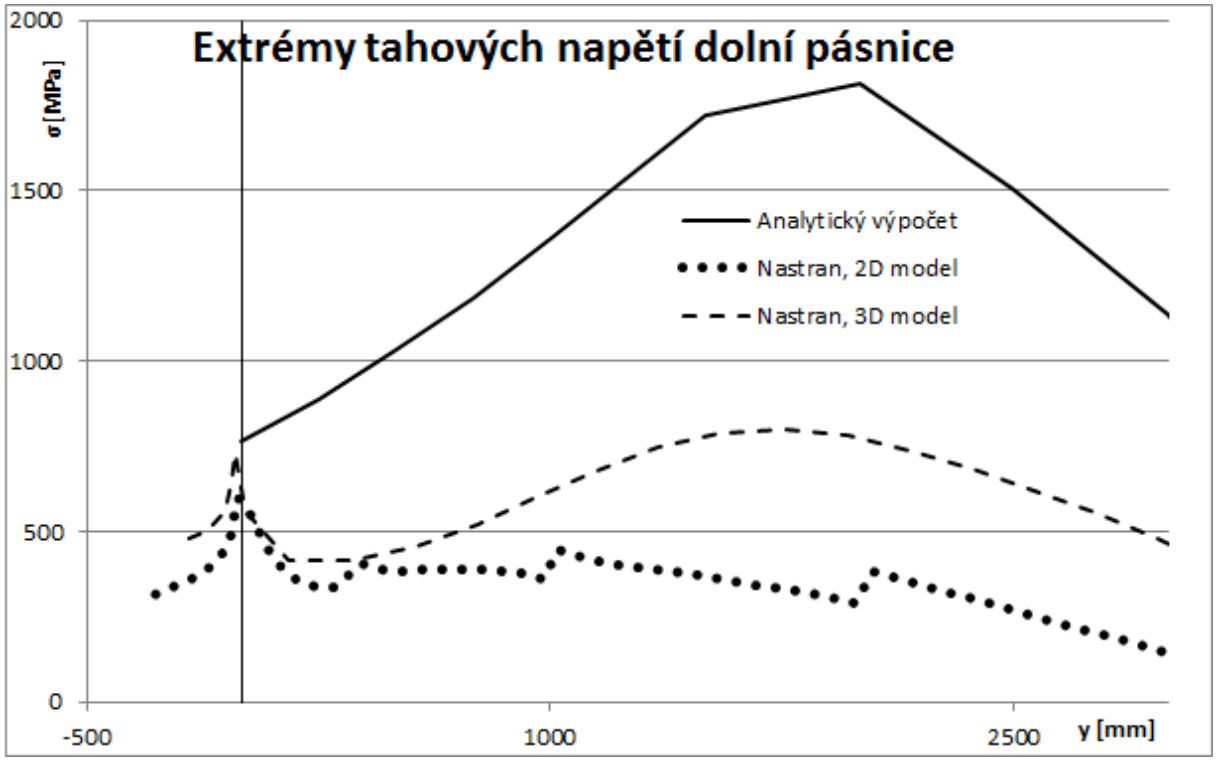

Graf 2: Průběh tahových napětí dolní pásnice.

Předchozí grafy znázorňují průběh napětí po rozpětí. Je zřetelně vidět vstupní předpoklad, že největší podobnosti jednotlivých výpočetních metod nastávají právě v oblasti kořenového žebra. Pro lepší přehled o napjatostním stavu v této oblasti slouží následující grafy:

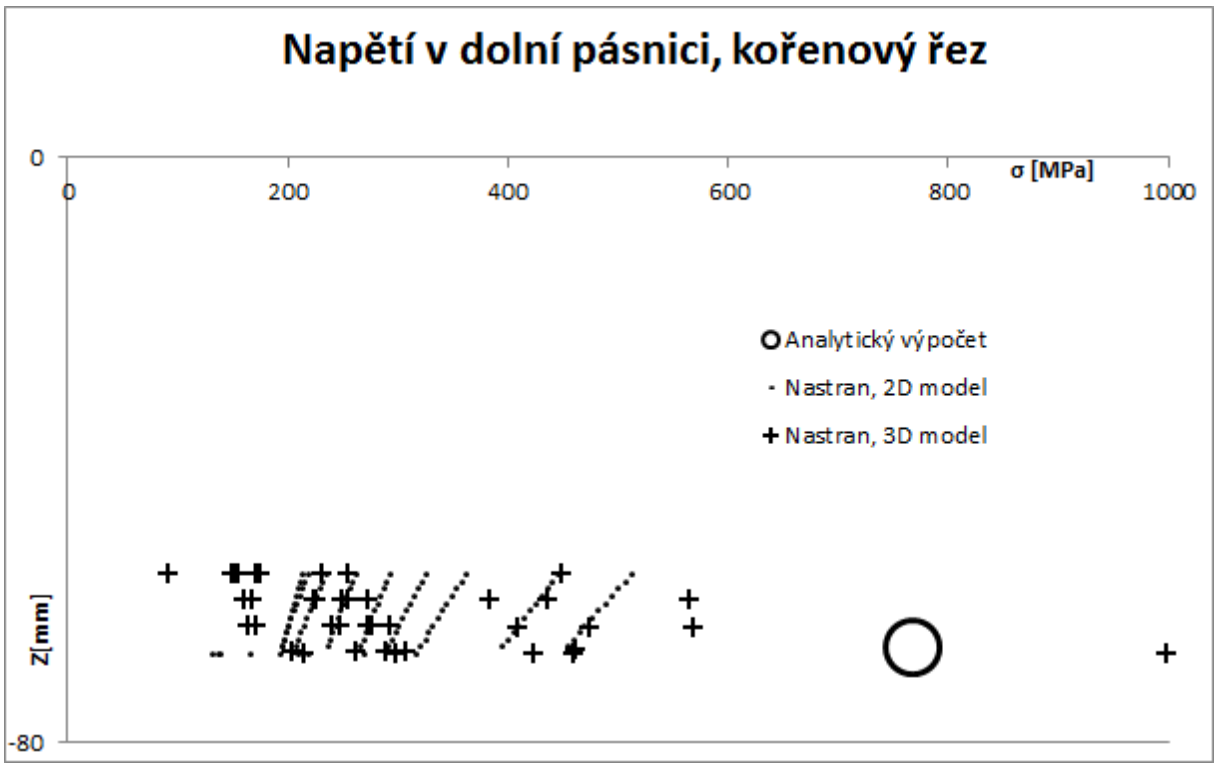

Graf 3: Rzložení tahových napětí v dolní pásnici v kořenovém řezu.

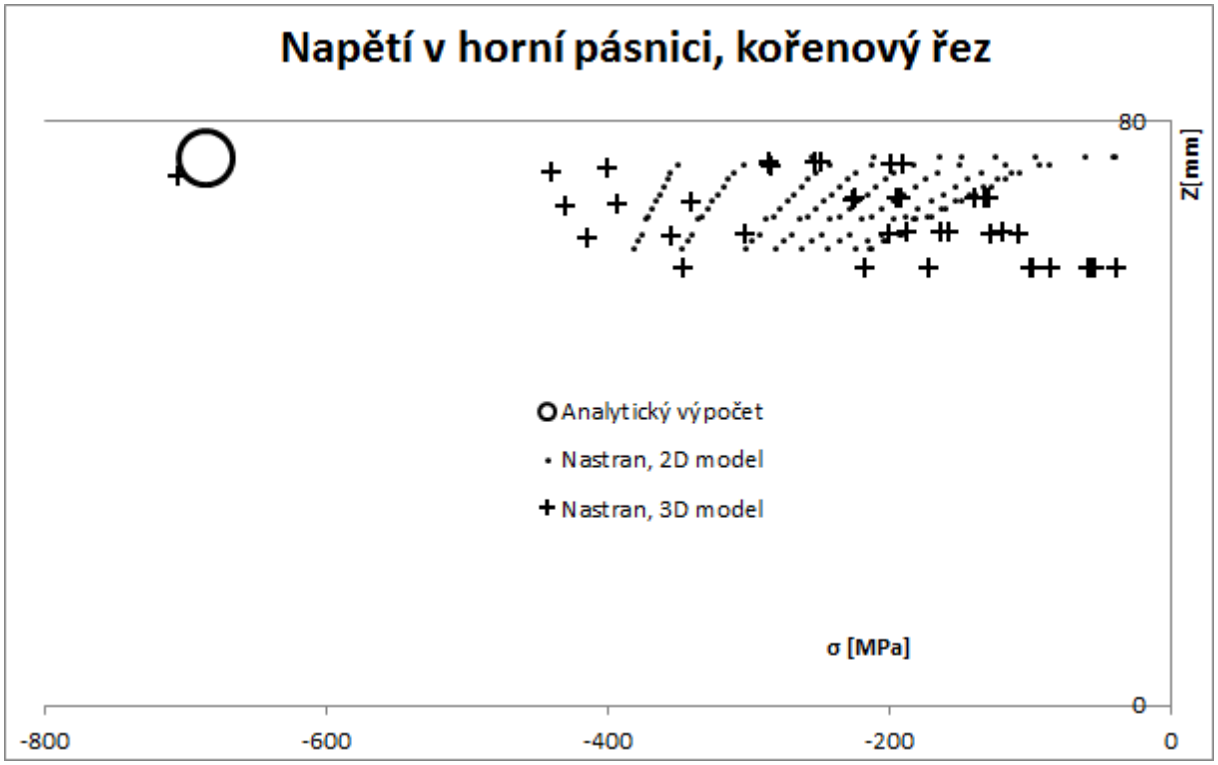

Graf 4: Rzložení tlakových napětí v horní pásnici v kořenovém řezu.

V těchto grafech je znázorněn napěťový řez pásnicemi v oblasti kořenového žebra. Na vertikální ose je výšková souřadnice pásnice a na horizontální ose je odpovídající napěťový stav. Poloha extrémních napětí velmi přesně odpovídá predikovaným hodnotám a polohám analytického výpočtu.

Analytický výpočet extrému napětí se shoduje s výsledkem 3D modelu pro horní pásnici podstatně lépe než s dolní pásnicí. Tento drobný rozdíl je způsoben rozdílnou geometrií: horní pásnice je téměř rovná a skutečně má charakter přímého nosníku. Zatímco dolní pásnice je mírně zalomená směrem vzhůru.

4 Závěr

Během modelování byla sestavena metodika přenosu komplikovaného vrstvení do vlastností konečnoprvkového modelu. Došlo k odzkoušení různých druhů modelů a kombinací okrajových podmínek a zatížení a jejich vliv na konvergenci řešení, deformaci a napjatostní stav.

Na základě provedených simulací lze sestavit několik pravidel, podle kterých se budou řídit příští návrhy a analýzy kompozitních křídel:

- nelze zanedbávat dopředný ohyb křídla,
- nutno zohlednit velké provozní deformace křídla,
- simulace pomocí 2D elementů není dostatečná.

Jako nejvýznamnější přínos dosavadní simulace je poznatek o důležitosti ohybové tuhosti nosníku v dopředném směru. Je nutné využívat široké pásnice s vysokým kvadratickým momentem i ke druhé ose.

Jako další krok v analýze segmentu kompozitního křídla budou provedeny:

- vyhodnocení napěťových stavů pomocí pokročilých poruchových kriterií Puck a Larck,
- analýza vlivu vyztužené náběžné hrany sloužící jako další nosník,
- analýza vlivu tuhosti kořenového žebra,
- přidání kontaktních vlastností mezi lepidlo a okolní konstrukci.

Reference

[1] Matěják V. LU04-2010-304ZK_R1 Test methodology-G304 S wing. VUT Brno, 2010

[2] HPH. Geometry report, 304S-0710-001 RA.02. 2010

[3] Juračka J. LU15-2007-ARC.ST Referenční statická zkouška segmentu křídla, VUT Brno 2007

[4] MD Nastran R3: Quick Reference Guide, 2008 MSC.Software corporation.

[5] MD Nastran R3: MD User's Guide - Application Examples, 2008 MSC.Software corporation.